7/5/96

On the Global Transport of Moisture: Comparison of Different Estimators

R. Haskins, E. Fetzer
Ca ifornia Institute of Technology / Jet Propulsion Labora ory
4800 Oak Grove Drive, Pasadena, CA 91109

T. Barnett, M. Tyree
Scripps Institute of Oceanography, 'University of California, San Diego

E. Roeckner
Max Planck Institute for Meteorology, Hamburg, Germany

6/ 10/96

Abstract

An intercomparison is made between vertically integrated water vapor flux estimates from the NASA reanalysis product, and from two versions of an atmospheric general circulation model (AGCM) forced only by observed sea surface temperature (SST). The period of comparison was from March 1985-February 1991 plus data from the U.S. flood in 1993. Time series from all three gridded fields are compared with simultaneous estimates of moisture flux directly observed by radiosondes. The temporal structure of the assimilation or reanalysis is similar to that of the radiosondes, leading to large correlations between these two fields as one would expect. However, it is shown that the assimilation is no better, and in certain cases worse, than the climate models on interannual scales.

Five year average maps of water vapor flux are broadly similar among the three model products, particular] y between the two AGCMS. The zonal averages of these maps have only small differences, both between datasets examined here and when compared with earlier studies based on interpolated radiosonde data. Nevertheless, maps depicting differences between the five-year-averaged assimilation and SST-forced AGCMs indicate local deviations as large as 50°/0 of the flux magnitudes. It may be noted that reanalysis products from different groups also have differences as large. in the present case, the AGCMs show a stronger current of water vapor that extends equator-ward on the western edges of all continents and into the subtropical trade wind belt. In monsoon areas of southeast Asia and central America, however, the models have relatively weaker moisture flux fields. Difference maps indicate that the assimilation has general weaker fluxes than

the AGCMs throughout the subtropics. The zonal average zonal fluxes are all similar, matching earlier estimates.

Season averages over the five year records examined show broadly similar structures between models and assimilation, but AGCM flux magnitude was often larger by as much as 50?4. These spatial similarities are manifested in the first EOFs, which arc similar between all fields and dominated by a strong southeast Asian monsoon. Smaller scale features, e.g. the nocturnal jet over the central and southern United States, are surprisingly well captured by the AGCMs, a result we did not expect..

An examination of the ENSO signal also shows broad agreement between assimilation and models, with significant differences occurring mainly over data-sparse regions in the Indian Ocean. 'l-he SST-forced AGCMs reproduced well the observed reduction in moisture flux observed over the United States during the drought of 1988, but not the observed changes during the flood period of 1993. Apparently other physical processes were responsible for this latter event. Finally, all of the estimates of moisture flux show large influxes of fresh water to the region of the Ross Sea. It has been shown that such fluxes in this critical region are important in modulating the ocean's thermohaline circulation, and so must be included in any model of this latter phenomenon.

1. Introduction

It has become increasingly apparent over the last decade that an accurate description of and ability to numerically model the global hydrological cycle is critical to understanding and predicting future climate change (Chahine, 1992). This is true on time scales of expected Greenhouse effects, as well as on shorter time scales, e.g., those associated with 'events' such as individual droughts and floods, changes in precipitation patterns associated with interannual ENSO, and decadal variability.

The transport of moisture by the atmospheric circulation is one of the most difficult aspects of the hydrological cycle to observe and hence, to model. This is partially because one needs two different three-dimensional fields to compute the transport (velocity and specific humidity). Further, these required fields are normally measured only by radiosonde stations, which are located mainly on the continents and scattered islands. Thus, over the vast ocean areas, which make up the majority of the planetary surface and are the major source of moisture, there are no direct observations of atmospheric moisture transport with which to verify models. Indeed, it appears there has been little effort to date to see how well atmospheric general circulation models (AGCMs), the models used for Greenhouse scenario runs and global climate predictions, actually simulate the moisture transport by the atmosphere. With this in mind, the basic goal of this paper is to test the ability of two AGCMs, forced only by observed global SST, to reproduce the moisture transport by obtained by a modern assimilation product and the traditional radiosonde network. We will concentrate on the mean and annual cycle of the transport. although a brief study of interannual variability will be included.

Before conducting the intercomparison, it is valuable to review the history of attempts to estimate global water transport. The pioneering efforts of Starr and Peixoto (1958) and Rasmussen (1966, 1967, 1968) used a spatially limited set of relatively short radiosonde station data to estimate the transport over North America. Hastenrath (1966) conducted a similar study over the Gulf of Mexico and Caribbean regions. These studies were extended to the Northern Hemisphere by Rosen et al. (1979) and globally by Peixoto and Oort (1983) as more complete radiosonde data sets became available. The same station data were used to make preliminary, regional estimates of the interannual variability in moisture transport by Peixoto et al. (1981).

In recent times, the analyzed products of national weather services have been used to revisit some of the above studies. Newell and Zhu (1994), whose imaginative work sparked our interest in the subject, used the ECMWF products to show the distribution of moisture transport in the Northern Hemisphere and its possible impact on paleoclimatic history obtained from icc cores. Matsuyama (1992) used the ECMWF analysis to study transport over the Amazon Basin. In perhaps the most ambitious study of its kind to date, Roads et al, (1994), used the NMC analyses

and other types of data to try to balance the water budget of the conterminous United States. While the usc of a consistently analyzed set of weather products seems the way to proceed with such studies, the work of Wang and Paegle (1995) and Mo and Higgins (1996) shows clearly that different, credible analysis products yield differences in transport estimates that are unacceptably large, even over North America where there is a spatially dense set of direct observation.

It is from this base of study that we will endeavor to explore the global water transport estimates from AGCMS, an analyzed data set that has blended into it a large and unique set of satellite and in situ data, and direct estimates from raw radiosonde observations. Section 2 describes the different tools for estimating the moisture transport. Section 3 provides an overview of the different estimates of transport, while Sections 4 and 5 inspect the different estimates on selected space and time scales. The interannual variability of the transport, as it relates to a subset of real climate problems is addressed in Section 6. Section 7 summarizes our work.

2.0 Data and Models

This section describes the models, assimilation and radiosonde data sets used in this paper. The descriptions are deliberately brief, as extensive references (given below) already exist in the literature.

a. Atmospheric models

The first atmospheric general circulation mode] (AGCM) used in the study is the European Center Hamburg Model (ECHAM3) developed at the Max Planck Institute for Meteorology in Hamburg. The model data used in this study were obtained from a 10-year-long T42 resolution run made using specified sea surface temperature (S S3'), i.e., the Atmospheric Model Intercomparison Program (AMIP) runs (Gates, 1992). This version of the model had 19 levels in the vertical, prognostic cloud water content and other advanced physical parameterizations. A full description of the model maybe found in Roeckner et al., 1992.

The ECHAM3 model deals with convective and stratiform clouds separately. It uses a comprehensive mass flux scheme for cumulus convection (Tiedtke, 1989). The cumulus convection scheme comprises the effect of deep, shallow and mid-level convection on the budget of heat, water vapor and momentum. Cumulus clouds are represented by a bulk model including the effect of entrainment and detainment on the updraft and downdraft convective mass fluxes. Mixing due to stratocumulus convection is parameterized as a vertical diffusion process (Tiedtke et al., 1988) with eddy diffusion coefficients depending on the cloud water content, cloud fraction and relative humidity jump at cloud top.

The second model used in this study is a newer version of the above model, ECI 1AM4 (Roeckner, et. al., 1995). This model shares many of the advanced physical features of its predecessor. Significant differences include a new radiation scheme and improved land surface characteristics. The most important difference is that the advection of moisture in ECHAM4 is by way of a semi-1.agrangian technique (Williamson and Rasch, 1994).

b. Goddard Data Assimilation Model (DAO)

The Data Assimilation Office (DAO) at the Goddard Space Flight Center has produced a multi-year global assimilated data set with version 1 of the Goddard Earth Observing System Data Assimilation System (Schubert et al., 1993). The two main components of the data assimilation scheme are a AGCM and an optimal interpolation (01) analysis scheme. For the multi-year assimilation, the AGCM was integrated on a 2° latitude by 2.5° longitude resolution with 20 sigma levels in the vertical. The AGCM is described by Takacs et al. (1994), Suarez and Takacs (1995) and Molod et al. (1996). The analysis scheme is described by Pfaendtncr et al. (1995). The salient features of the two pieces of the system are described very briefly below.

The Tropospheric version of the Goddard AGCM uses a potential enstrophy and energy conserving horizontal differencing scheme on a C-grid. An explicit leapfrog technique is used for time differencing, in which an Asselin time filter is applied to damp out the computational mode. An eighth-order Shapiro filter is applied to the wind, potential temperature, and specific humidity at every step. The model uses the vertical finite differencing scheme due to Arakawa and Suarez. Penetrative convection originating in the boundary layer is parameterized using the Relaxed Arakawa-Schubert technique. Negative values of specific humidity produced from the finite-differenced advection arc filled by borrowing from below. This version of the AGCM was run without a land surface model. Soil moisture was computed off-line based on a simple bucket model.

The 01 analysis scheme employed by the data assimilation model scheme has a horizontal resolution of 2° latitude by 2.5° longitude resolution of 14 pressure levels. Analysis increments are computed every 6 hours with a 3 hour data window. Upper-air analyses of height, wind, and moisture incorporate data from rawinsondes, dropwindsondes, rocketsondes, aircraft winds, cloud tracked winds and thicknesses from the NOAA/NESDIS TOVS soundings, The 01 scheme is multivariate in geopotential height and winds and employs a damped cosine function for the horizontal correlation of model prediction error. The height-wind cross correlation model is geostrophic and scaled to zero at the equator, The multivariate surface analysis scheme adopts an Ekman balance for the pressure-wind analysis. The moisture analysis employs only rawinsonde data. There is no initialization scheme in the assimilation system, which relies instead on the

damping properties of a Matsuno time differencing scheme and by an incremental Analysis Update procedure,

c. Radiosonde Data Set

The DAO assimilation and the ECHAM3 and ECHAM4 models were validated against a set of approximately 40 radiosondes distributed around the globe. These stations and their location are listed in Table 1; their geographical distribution can be seen in figures 1 through 3. The validation data set consists of time series of vertically integrated water vapor flux estimated with the radiosonde observations at the standard times of O and 12 Universal Time. These series are compared with series of DAO assimilation or ECHAM model Q-fluxes at the nearest representative gridpoints.

The radiosonde vertical integrals for most stations were calculated from observations at the surface, and appropriate pressures of 1000, 950, 900, 850, 800, 700, 600, 500 and 400 mb. At high latitudes the 400 mb humidity is frequently missing, so Q-fluxes from stations in the far northern Pacific did not include this pressure. It was found that many additional stations showed significant data dropout when 300 mb was included, thus determining the standard 400 mb cutoff. The 950 and 900 mb observations were absent from the South African stations, so these pressures were not used in calculating the integrals in this region. Quantities used in the integrals include relative humidity, temperature (for converting relative humidity to specific humidity), and wind speed and direction. If any of these quantities is missing at any pressure value and time step, the integral (see below) is not calculated and the flux then is flagged as missing. With this criterion the radiosonde time series are usually more than 95°/0 complete; many stations yield series that are more than 99°/0 complete.

d. The Vertical Integrals

The physical field of interest in this work is the total water vapor flux This vertically integrated quantity is defined as

$$\underline{Q} = -\frac{1}{g}\int_{p_{surface}}^{p_{top}} (\underline{u})q\,dp$$

where q(p) is the specific humidity at pressure level p, (u(p), v(p)) the zonal and meridional components of the velocity at level p, g is gravity, and the vertical integral extends from the surface to an upper limit. This limit is the model top in the ECHAM anti DAO fields, and 400 or 500 mb in the radiosondes (as discussed above). The estimate of the integral is insensitive to the selection

of upper level, since there is very little moisture above 500 mb. We refer to this vertically integrated moisture flux as the Q-flux. It is calculated for each of the data sources discussed above.

3.0 DAO and ECHAM assessments

Before comparing AGCMS and DAO products, it is necessary to see how well DAO matches some of the original observations that went into its construction. It is also important to compare the ECHAM simulations with observations at seasonal and longer time scales, where climate models might be expected to best match observations. Wc selected the raw radiosonde data set as a 'ground truth' against which to measure the reliability of DAO at all time scales, and of ECHAM at longer time scales. Although other types of data went into the DAO, we felt the sondes were the most direct atmospheric observation, and the most important. The radiosonde locations used in this study are shown in Table 1.

a. Global distribution of correlation

The method of directly validating the DAO assimilations, the ECHAM3 model, and the ECHAM4 model against radiosonde observations was as follows: first, time series of Q-flux at DAO / AGCM gridpoints nearest to a radiosonde station were constructed. The gridded field Q-flux time series were then matched with the associated radiosonde station Q-flux time series. These series are referred to as companion pairs: there are three companion pairs at each radiosonde station. The temporal correlation between companion pairs over the period March 1985 through February 1991 was then constructed, (This is the longest continuos data set available at this writing, and the period analyzed in the rest of this work.) The Q-flux vector was treated as a complex number such that $Q = Qu + iQv$, where (Qu,Qv) correspond to the transport associated with the wind vector components (u,v). Hence the cross correlation between any two flux series is a complex correlation, $r = r_r + ir_i$, characterized by its magnitude $|rr^*|$ and phase angle $= \tan^{-1}(r_i / r_r)$. In the correlation calculations the radiosonde series are treated as reference, so the complex conjugate companion DAO or ECHAM series are used. By this definition, the conflation between a complex series and itself is identically unity. The correlations were calculated after passing the series through boxcar filters; the filter essentially removes sinusoids of periods equal to or shorter than its width. The result is correlation magnitude and phase that varies with filter width and station location. A close examination of the quantities discussed below showed no major differences between ECHAM3 and ECHAM4. So, we will compare the DAO performance only

with ECHAM4, with the knowledge that ECHAM3 conclusions are essentially the same as those of ECHAM4.

As might be expected from the nature of the assimilation process, the correlation is strongest in the unfiltered DAO companion pairs. This is an indication that the DAO assimilation captures the dominant variability of the water vapor transport in the radiosondes at shorter time scales. The diurnal, semiannual and higher frequency modes arc all well represented in the DAO estimates. In contrast to the radiosonde-DAO pairs, the poorest correlation is seen in the unfiltered radiosonde-ECHAM companion pairs -- typically .1 or smaller, The effect of smoothing on radiosonde correlations with both DAO and ECHAM is illustrated for a few typical cases in figures 1and 2, which shows correlation magnitude as a function of filter width at Dodge City and Curacao (typical of midlatitude continental and tropical maritime conditions, respectively), There are several significant lessons to bc learned from the curves in figures 1 and 2. First, the gradual decrease in the DAO correlations suggests that events at all scales arc well characterized in the assimilation, but that short scale events are best characterized. Secondly, the increase in the ECHAM4 correlations with filter width shows that the model can describe well the flux events over seasons to years. Finally --and most importantly -- the DAO correlations at longer filter widths are only slightly higher than those of the ECHAM4. These results suggest that the DAO flux variability at shorter periods is determined directly by the observations, but flux variability at longer periods is more dependent upon model physics and the specified SSTs. At climatological time scales the DAO assimilation fares no between at characterizing the water vapor flux observed by the radiosondes than do the ECHAM models, with both presumably determined by model physics and SST boundary conditions

These arguments can be extended more globally. Figure 3 is a map of DAO correlation magnitude and phase for unfiltered series (the comparable ECHAM4 correlations are not shown because they are negligible). For comparison figures 4 and 5 are maps of correlations between radiosondes and both DAO and F, CHAM4 after smoothing with a 400 day-width filter. Again, the best correlation is seen with unsmoothed radiosonde-DAO companion pairs in Figure 3. After smoothing with the 400 day-width filter, however, the DAO correlates with the radiosondes only slightly better than does ECHAM4. Again, this suggests that at climatological periods of roughly one year or longer the sea surface temperatures and model physics are the major determinants of the flux behavior, The observations impart the assimilations no significant improvement over the SST driven models at climatological time scales.

b. Estimator biases.

A second measure of model validity is bias between the gridded fields and the radiosondes. This quantity is estimated by calculating the five-year average flux for each companion pair at the

radiosonde stations. Converting the magnitudes to percentage deviation of DAO or ECHAM4 from the radiosondes and mapping the results gives an overview of the biases. These results are presented in Table 2. To summarize, the ECHAM4 percentage biases are typically positive and of greater magnitude than those of DAO. The largest biases in the ECHAM4 fluxes are found in the far north Pacific, While DAO is less biased, it consistently underestimates the radiosonde fluxes magnitudes; DAO fluxes were larger than the radiosondes' at only 8 of the 38 stations examined. The relative magnitudes of these biases should be kept in mind when the DAO and ECHAM fields are compared.

c. Summary

The above tests, plus others discussed in Fetzer et al. (1996), suggest that DAO has at least three distinct regimes of behavior: accurate short period transient events; less accurate, but adequate seasonal accuracy; and poor interannual accuracy, This conclusion is in fact supported in the DAO documentation itself Molod et al. (1996). These results are also demonstrated later in the text in the comparisons of different time period events.

Since no data set can be used as absolute 'truth', the remainder of the paper compares the three data sets based on phenomenology.

4.0 Annual Mean Moisture Transport

The purpose of this section is to briefly describe the major features of the annual mean global Q-flux field obtained from the DAO and the two AGCMs. The degree of similarity (or lack thereof) between these features as they appear in the three estimates is discussed next with several estimates of the key differences being presented.

a. Description

The annual mean moisture transport computed over the five year period 1985-90 from the two AGCMS and the DAO are shown as vector quantities in Figure 6. In this illustration all vectors are scaled identically. In general, all estimates of the annual mean moisture flux appear in good agreement, consistent with remarks by Gates (1995) regarding mean annual conditions. There are a number of interesting features in this illustration that are shared by all three Q-flux estimators:

i) The strong northeastward moisture transport off the eastern margins of the northern Hemisphere continents is clear, a result in agreement with earlier results, e.g., Newell and Zhu

(1 994) and their discussion of 'tropospheric rivers'. These transports obviously provide much of the moisture for western N. America and Europe.

ii) The tropical Atlantic, even far into the S. Atlantic for the AGCMs, provides much of the moisture for both Central America and the Amazon. The latter result is in agreement with that of Matsuyama (1992).

iii) The Pacific Trade Wind System transports large amounts of water vapor westward to meet an eastward transport from the Indian Ocean, resulting in a large Q-flux convergence over the west Pacific warm pool and southeast Asia.

iv) The circulations out of the subtropical southern Indian and Atlantic oceans curve over the African and S. American continents. respectively, but then return seaward, ultimately depositing moisture in the high latitudes of the southern oceans and Antarctica.

v) The strong Antarctic circumpolar moisture flux in the 'roaring 40s' is well captured in all three models.

vi) Many of the small scale features of the Q-flux field are common to all three estimates. For example, the flow of moisture out of the Gulf of Mexico into the United States midwest and, subsequently, out over the east coast is obvious in all three estimates, The same may be said for the narrow 'rivers' that run over northern Australia and over southeast Asia.

An interesting feature of the annual Q-flux over much of the globe is its close relation with and dependence on the positions of the subtropical high pressure features over all three oceans, a result that will stand out even more clearly in the discussion of the seasonal cycle of Q-flux. These senli-permanent high pressure systems must be well reproduced by AGCMs if the models arc to faithfully represent the global Q-flux field.

b . Intercomparison

1). Zonal Averages

The traditional way of presenting the mean moisture flux involves zonal integration, as shown in Figure 7. The zonal integral of the zonal U-flux shows the DA() and AGCM distributions are all in good accord. l-he latitudes of peak transport are in excellent agreement among the three model estimates, as are the magnitudes of the transport that generally are within 10% of each other. Note however that the JDAO consistently underestimates the flux compared to the AGCMs. Other integrals of the moisture transport (not shown) give similar results.

Inclusion of the older estimates of zonal flux by Peixoto and Oort (1992) in Fig 7 show those estimates, obtained from interpolated radiosondes only, differ substantially from the more physically based transport estimates. Note the older transport estimates peak at latitudes that differ from those of the other estimates by 1000 km or more, Further, the magnitude of the transport,

while in reasonable agreement in the northern and tropical latitudes where there are radiosondes, is different by 20-25% in the higher southern latitudes. This might have been expected for there are few, if any, observations in these latitudes upon which to base Q-flux estimates.

In summary, the integral properties, represented by the zonal average of the three modern estimates, are in good agreement with each other. They differ substantially from older estimates in data poor areas, where the interpolation schemes, based only on assumed statistics, are apt to be less reliable then the more physically based estimates of the models.

2). Global Distributions of DAO and ECHAM Differences

The vector difference maps between the DAO and the two ECHAM AGCMs were computed and are shown in Figure 8. The detailed picture of the transport offers some interesting and unexpected results. Inspection of these maps shows there are some large scale differences between the different estimators of the Q-flux but on the whole the agreement between the DAO and AGCMs is better than might have been guessed a priori. The main differences, keyed to the main features of the mean field presented above, arc discussed below:

i) The northeast flowing tropospheric rivers off the eastern edges of the northern Hemisphere continents is captured very well by the AGCMs, with typical differences being of order 15°/0. The sense of the differences is that the AGCM transport is stronger, especially over the Atlantic. The agreement is about as good as onc could expect; especially over ocean areas with few direct observations.

ii) The Q-flux into the Amazon and central America is again stronger in the AGCMs, especially over the tropical Atlantic. The actual flux estimates over the continent are also stronger, but the difference signal is somewhat irregular in space.

iii) Both AGCMS show substantially higher estimates of the moisture transport in the Pacific Tradewind System compared to the DAO. The differences in some regions are nearly 50°A of the long term mean flux and that is due, in part, to an underestimate by the DAO (Mo and Higgins, 1996). This is also implied by Lau et al. (1995) in an evaporation minus precipitation comparison among 23 AMIP AGCMS. In that study, EC} IAM3 compared quite favorably to two in situ data sets, while the DAO underestimates the in situ data by about 50°/0.

iv) The circulation over the eastern parts of central and southern Africa is somewhat weaker in the AGCMS than in the DAO. This is especially true in the ECHAM4. In fact the AGCMs generally have weaker transport over much of the Indian Ocean than does the DAO. In regions near the west coast of southern Africa, however, the ECHAM transports arc notably stronger than DAO transports. The curving circulation over S. America is in better agreement among the estimators.

v) The small scale features are rather well reproduced by the AGCMs. Over the central US the flow is slightly too strong but the differences are of order 20%. The transport over northern Australia and southeast Asia seems well reproduced by both AGCMs

Perhaps the most surprising aspect of our study so far is the high degree of similarity between the two AGCMs. Inspection of Figure 8 shows their disagreements with the DAO, where they occur, are nearly identical. The only major differences occur in the Southern Hemisphere in circumpolar transport, off the southeastern coast of Africa, and the central southern midlatitude Pacific. This was unexpected due to the radically different manner by which the AGCMs advect moisture (see Section 2.1). For all practical purposes the mean transport fields of the two AGCMs are identical. If other variables had been examined at selected altitudes and latitudes the differences would likely have been much more dramatic (Rasch, personal communication).

5.0 seasonal Cycle of Moisture Transport

This section examines the seasonal cycle of moisture transport as it appears in the two models and DAO. The comparison is done first through zonal mean plots, then seasonal vector plots as those used in the previous section. Next wc investigate the seasonal cycle by way of the complex empirical orthogonal functions (CEOFs; Barnett, 1983) of the full Q vector. This approach allows the presentation of both magnitude and phase of the seasonal cycle on the same illustration. As wc shall show, this also allows a more quantitative comparison of the agreement between the AGCMs and DAO. The CEOF analysis was done on 30 day averages of the original signals to suppress synoptic variability but was checked on 5 day averages as well.

a. Zonal Averages

The zonal averages of the zonal transport for winter (Dee-Jan-Feb) and summer (June-July-Aug) are shown in Figure 9. The difference between the physically based estimates and those based on statistical interpolation are more pronounced than were seen in the case of the annual mean. This is especially true in the tropics and high southern latitudes where the older estimates miss or misplace important features in the zonal moisture transport. Indeed, it is remarkable these latter estimates come as close as they do to the modern values considering the paucity of data upon which the Peixoto and Oort (1991) estimates were based.

For purposes of intercomparison, the use of the zonal mean display of Fig 9 is relatively uninformative, since all physical estimators appear somewhat similar. This is at first glance highly encouraging, but in fact zonal integration hides significant regional differences, as we shall see

below. One feature that is suggested by Fig. 9 is that ECHAM3, and especially ECHAM4, have stronger season cycles than either the DAO or the estimates of Peixoto and Oort.

b. Physical space description

The seasonal variations in Q-flux arc shown in Fig. 10 for the winter season (Dee-Jan-Feb) and Fig 11 for the summer season (June-July-August) to illustrate their global characteristics in physical space. Because the performance of the two AGCMS is so similar, we show only the Q-flux from ECHAM4. The discussion is organized around the seasonal behavior of the main features of the annual mean cycle (Section 4.1) to offer a different aspect of the seasonality than seen by the CEOF analysis to follow:

(i) The strong northeastward transports off the east coasts of Asia and North America are stronger and penetrate the continents more deeply during the winter (DJF) than summer (JJA). During this season, the main flow is also displaced eastward from the coast. During summer the flow closely hugs the land-sea boundary, a result likely due to the eastward displacement of the Pacific and Bermuda high pressure systems.

(ii) The Q-flux from the Atlantic is more zonal in the winter hemisphere, but has substantially more curvature in the summer hemisphere. This is apparently because the subtropical highs in the North and South Atlantic reach maximum strength in their respective summer season anti so have stronger anti -cyclonic circulation then. In either season. the Amazon still receives a net influx of moisture from the Atlantic, while the transport over southern portion of South America is eastward.

(iii) The tropical Indo-Pacific shows the most striking examples of seasonality. It is this feature that dominates the CEOF analysis discussed below. During DJF, zonal flow from the Pacific penetrates into the Indian Ocean extending to east Africa. This flow is much larger than the small return flow to the Pacific just south of the equator, so during DJF the Pacific is exporting water, via the atmosphere, to the Indian Ocean region and beyond. During northern summer (JJA), the flow reverses so that the net transport in the tropical region is from the Indian to the Pacific. Both of these features are clearly linked to the seasonal reversal of the Monsoon System.

(iv) The South Atlantic and South Indian Oceans still provide moisture for the southern oceans and Antarctica but the fetch over which this moisture is acquired is displaced southward and shortened during the Southern Hemisphere winter compared to the summer.

(v) The smaller scale features of the seasonal] y varying Q-flux undergo large changes. I-or instance, the moisture jet over North America is strongest with greatest meridional extent in the local summer season. The Q-flux in the winter season appears more correlated to the subtropical jet that normally passes over the Gulf of Mexico and southeastern United States at this time of

year. The small scale jet that brings moisture to eastern and northern Australia is clearly seen in the local summer (DJF) but has shifted so farnorth inthewinter (JJA)asto have no impact on the continent.

The AGCMs and the DAO capture all of these features and temporal characteristics. The major difference being that the ECHAM Q-flux is somewhat stronger compared to DAO; note the relative vector lengths in Fig, 10 and 11. Vector difference maps (not shown) place the largest differences in the tropics.

In summary, the moisture flux in the atmosphere undergo strong seasonal changes. The most dramatic of these is the seasonal reversal of the exchange of atmospheric moisture between the tropical Indian and Pacific Oceans and between the tropical Atlantic and Pacific Oceans. Other, smaller scale features, such as the moisture jet over the central and eastern United States, can disappear or be strongly altered with season.

c. CEOF description

All three CEOF analyses, based on one-month averages of the five years of raw data and shown in Fig. 12, place the maximum variability around the Monsoon System. Associated with these first modes is 37-410/0 of the variance, depending on estimator; the second and higher modes arc statistically degenerate using the criteria of North et al. (1982). A pronounced anticyclonic circulation in the north Pacific is seen in all three fields in Fig. 12. In the subtropical Pacific this pattern is directed opposite to the Monsoon signal in all three estimates, reflecting their six month phase difference. This north Pacific signal is somewhat stronger in ECHAM4 than the other two estimates.

Other features seen in Fig. 12 are not as unambiguous as the two just discussed, Both AGCMs produce a moderate secondary signal over central America that is in phase with the southeast Asian Monsoon signal. while DAO gives only a suggestion of this feature. Similarly, both models produce an anticyclonic signal in the north Atlantic, but this feature is much weaker in the DAO. Note also the pronounced feature in the south Pacific in the ECHAM4; this feature is far less apparent in either DAO or ECHAM3.

"The temporal amplitude and phase derived from the CEOF analysis are shown in Fig. 13. Both the amplitude and phase from the AGCMs have been obtained by projecting the AGCM data onto the DAO eigenvectors. The semi-annual signal in the amplitude shows the seasonal cycles to be strongest in the northern summer and winter, as one would expect from the patterns shown in Fig 12. The magnitude of the cycle (Fig 13a), in the DAO, is closely replicated by both AGCMS, although the ECHAM4 is given to occasional larger excursions than ECHAM3, e.g. summers 1987 and 1989 and a stronger seasonal cycle in general, just as we saw above. The temporal

phase of the seasonal cycle (Fig 13b) is virtually identical among the three estimates. What differences there are suggest that the DAO shifts from one phase (say O degrees) to the opposite phase (180 degrees) within a month, i.e. a complete reversal in the physical direction of the moisture flux similar to that seen in Fig. 10 and 11. The AGCMs generally do not make such abrupt shifts but rather require 1-2 months to shift from one phase of the Monsoon to the other, especially the transition from winter to summer conditions.

d . CEOF Intercomparison

Because the annual cycle is dominant in the amplitude of the first CEOF in assimilation and models, it easy to quantitatively evaluate the skill of the AGCMs to reproduce the DAO data. Several measures of comparison are given below:

i) As mentioned in the previous section, the leading CEOF captured 39.2% of the DAO Q-flux. The next two modes captured 6.7 and 5.4%, respectively, and were not statistically distinct. The first mode for ECHAM3 and ECHAM4 captured 37.4 and 4 12°/0 of their variance, respectively. Essentially, the fraction of variance captured by the leading modes was independent of Q-flux estimator. The second and third modes from the models explained virtually the same variance as did those from the DAO and had the same degeneracy.

ii) The inner product of the first DAO CEOF with the leading CEOFs from the models was 0.82 with ECHAM3 and 0.85 with ECHAM4. The complex phases associated with these correlations were 19.0° and 17,6°.

In summary, the spatial distribution and phasing of the seasonal cycles of Q-flux produced by the two AGCMs is virtually identical to that found in the DAO. The exceptions to this statement arc associated with extent and shape of the region of largest seasonal cycle, and in the strength of the secondary features of that cycle. In general, however, these secondary features are correctly located by the AGCMs.

6.0 Interannual Variability

The length of the synchronous time series presently available from the AGCMs and the DAO is too short to carry out any sophisticated study of interannual variability of their Q-flux. However, it is possible to get a qualitative impression on the intercomparison of this time scale of variation in the AGCMS and DAO by looking at several case studies. The three cases discussed below cover different types of climate situations from extreme events to ENSO impacts to more subtle features of the Q-flux field related to changes in the thermohaline circulation (THC) of the world's oceans.

a. Extreme Events: United States Drought/Flood

The United States experienced an unprecedented drought in the late Spring and summer of 1988 and a serious flood during approximately the same seasons in 1993. A nice description of the meteorological conditions contrasting these two extreme events can be found in Bell and Janowiak (1995). Physical mechanisms for these events have been suggested by Trenberth and Branstator (1992) describing the drought, and Mo et al. (1995) describing the 1993 floods. The former hypothesis included the distribution of anomalous SST in the Pacific, while the latter referred to more local forcing not related to SST.

How well did the AGCMS examined in this study simulate any changes that occurred in the Q-flux field that accompanied these two calamities? An answer is shown in Figures 14 where the anomalous Q-flux for May-June 1988 and is shown for DAO and ECHAM4. The anomalous Q-flux was calculated by differencing the two month average with the 7-year average monthly values. The ECHAM4 results were based on an ensemble average of 3 realizations of the Spring-Summer season, each starting from slightly different initial conditions (CF Barnett, 1995). The Pool-Pm-mutation Procedure (Preisendorfer and Barnett, 1983) was used to generate a cumulative distribution function from data over North America to test the mean (SITES) of the ensemble averages of 1988 and 1993. For a confidence level of greater than 97°/0 for the U-flux and 85 .5 °/0 in the V-flux. the two fields arc different and hence significant.

For May-June 1988, ECHAM4 shows anomalously low moisture transport into the interior of North America. The sense of the anomaly in the DAO is even stronger, suggesting a cessation of moisture flux altogether. Both signals are consistent with the drought pattern. The cyclonic and anti-cyclonic anomalous flows associated with the Bermuda High are shifted off the coast in the ECHAM4 and compressed. The most striking disagreement between the two Q-flux estimates is the very large transport associated with the equatorial counter current in the ECHAM4 that is almost non existent in the DAO data. In summary, both models suggest an important part of the drought mechanism was the lack of normal moisture flux from the Gulf of Mexico, an idea confirmed in numerous data studies. The production of this result from the ECHAM4, forced only with SST supports the premise of Trenberth and Branstator (1992).

The amplitudes of the moisture flux for DAO and ECHAM4 for the flood year of 1993 are presented in Figure 15. The amplitudes were shown in this case for an easier comparison of the results from the NCEP model as in Figure 15 in Bell and Janowiak, 1995. The NCEP model places the maximum amplitude of the moisture transport centered over Kansas, Oklahoma, and Missouri. The maximum for the DAO is found slightly northeast of the NCEP result, but is in fairly good agreement in pattern and magnitude. However, the ECHAM4 results indicate an

excessively strong jet associated with the moisture counter current off the coast of Central America that seems to disrupt the flow of moisture into the Gulf of Mexico and does not capture the excess flow from the Gulf of Mexico.

In summary, the AGCM did a reasonable job of reproducing key features of the moisture transport field during the drought of 1988. The performance during the flood of 1993 was not good. We hypothesize, as have others before us, that the former event was related to SST that were used to force the model and hence, its moderate success. The latter event is thought to have been more local in nature. The AGCM, with knowledge of SST only, would not capture such an event. (and it did not).

b. El Niño-Southern Oscillation (ENSO)

The tropical Pacific sea surface temperatures were unusually high during the winter of 1986-87 (El Niño) and unusually low during the winter of 1988-89 (la Niña) according to the Climate Analysis Center Bulletin. The Q-flux difference maps for the two winters for the DAO and ECHAM4 are shown in Figure 16. ECHAM3 results (not shown) agreed well with most of the features seen in ECHAM4, even though only one realization of each of these winters was available from each model.

The Q-flux vectors show that the South Pacific Convergence Zone shifted westward between the warm event to the cold event. The eastward shift of equatorial convergence from the central Pacific during the warm event to Indonesia during the cold event can also be discerned. The higher than normal pressure in the northeast Pacific and over the North Atlantic during cold events is especially clear on the difference maps (Fig 16b) where it appears as a anticyclonic circulation of the Q-flux. Less moisture penetrates the northern section of S. America during cold events, a feature associated with drought along the western coast of that continent. All of these features are well-documented properties of the ENSO cycle.

Comparing the difference maps in Fig 16 suggests the AGCM and the DAO have captured the principal features ENSO cycle. Over most of the globe, the warm-cold differences illustrated in Fig. 16 are virtually nil in both estimates suggesting no ENSO influence in these areas, as observed (e.g. Ropelewski and Halpert, 1987). The Pacific and Atlantic signals are well represented, although the AGCM has them slightly stronger than the DAO. The AGCM map does show an extra eastward jet in the tropical western Pacific not seen in the DAO. This is due to a latitude shift in the ECHAM mid Pacific moisture flux that is not found in the DAO. Also well represented is the reduced moisture flow into S. America from the Pacific during cold periods, and the suggestion of an anomalous high in the S. Atlantic,

The principal difference is in the southern Indian Ocean where it places a large El Nino response that is not in the DAO. 'I'he high latitude parts of the AGCMs Indian Ocean signal may be partially due to the fact we had only a single realization of the simulation. The low latitude part is more likely to be a real model flaw although there is not much data in this region upon which to base the DAO (see Barnett, 1995, for more on the latitudinal dependence of the model uncertainty).

In summary, the AGCM has done a surprisingly good job of producing warm/cold ENSO signals in the global atmospheric moisture transport field that agree well with those in the DAO.

c. Poleward Moisture Flux and the THC

Recent models of the global thermohaline circulation (THC) have shown the THC appears to be extremely sensitive to exchange of fresh water between the ocean and atmosphere (e.g. Pierce, et al. 1995). The vast majority of the models of the THC specify the fresh water flux to the ocean. A recent sophistication may be found in the work of Osborn (1995) who made the " exchange of fresh water a function of local ocean conditions, This raises the key question: Is it adequate to represent the crucial fresh water exchange as a 'local' process or is it necessary to account also for the advection of fresh water from higher latitudes to the regions of deep water formation in the southern Hemisphere'? If the latter is the case, then this transport must be included in THC models for it will surely change as the global climate changes in response to THC changes.

Our analysis of the Q-flux provides a clear answer to this question. The Poleward transport across 60S is shown in Figure 17. The DAO and AGCMs are in general agreement and show weak Poleward moisture transport at all longitudes, except in the longitude band of the Ross Sea (about 1 SOW) where the transport is roughly three times larger than at other latitudes. The Ross Sea was the region where Pierce et al. (1995) showed that small variations in fresh water flux to the ocean have a dramatic impact on the THC. Apparently the atmosphere is putting the water into just the region of the THC where it will have the largest effect.

Another view of the transport into the region of the Ross Sea is shown in Figure 18 where the Q-flux across the four boundaries of a box defined by latitudes 60S to 75S and longitudes 165E to 135 W is given. Almost all the transport comes from the northern boundary of the region, i.e. across 60S. The time series of the net transport into the box (Fig. 19) shows the region is usually receiving water from the north and hence precipitation exceeds local evaporation. The time series, although short, exhibits no ENSO or quasi-decadal signal: it appears more like white noise. A longer simulation would be needed to verify this suggestion.

In summary, there is substantial import of water by the atmosphere to the high latitudes of the southern Hemisphere, especially the Ross Sea. The sensitivity of present THC models to fresh water inputs to the ocean in this region implies that the such models are currently inadequate.

Their physics must be improved to include the moisture import and any dependence and/or feedbacks it may have on climate-induced changes in the THC itself. Failing this, the models omit a potentially key component of the THC physics.

7.0 Discussion and Summary

This study has compared global estimates of water vapor (Q-)flux from 1) a data assimilation procedure and 2) two versions of a general circulation model forced only by observed monthly mean, global sea surface temperatures. These estimates were also compared with directly observed Q-fluxes from a radiosonde network, and with earlier zonally averaged zonal fluxes.

The best overall correspondence in all these quantities was, not unexpectedly, between radiosondes and the assimilation (which were partially generated with those radiosondes). There was also good agreement between zonally averaged zonal fluxes and similar quantities from previous studies. More detailed maps of the five year average fluxes revealed some consistent differences. Most notably, the time-average oceanic subtropical DAO fluxes are weaker than their ECHAM model counterparts (problems with the DAO subtropical winds have been noted elsewhere Mo and Higgins. 1996). It was also surprising to find that the amplitude of the annual cycle of the Q-flux in the DAO was substantially less than that in the radiosonde data in the locations we investigated.

The five year average Q-flux from the ECHAM models arc remarkably similar, despite major difference in model physics. Most notably, the water vapor transport parameterizations were changed radically between ECHAM3 and ECHAM4 -- yet the time average flux fields change only slightly. Seasonal variations are the most significant difference between assimilation and models. These variations are only barely apparent when zonal average zonal fluxes arc compared. Seasonal average maps reveal a more complex picture. Models and assimilation have broadly similar structure, but the models show a relative increase in nonzonal features. This is true of both the December-January-February and June-July-August periods. Despite these qualitative seasonal differences, the annual cycle in all estimators have nearly identical first CEOFs (higher order CEOFs are statistically insignificant in all cases). This is primarily due to the magnitudes of both the southeast Asian monsoon signal, and midlatitude ocean regions that are phased opposite to the monsoon in the northern hemisphere. There are many secondary features in the first CEOFs that are intriguing but not coherent across all three estimators, suggesting geophysical noise.

The interannual variability of ECHAM4 and DAO were compared, and it was seen that they showed much different character the summer 1988 drought and the flood year Of 1993 over the United States. This appeared related to relative strong Bermuda high in the ECHAM models at this time and to the fact that the drought has been related to the global SST (used to force the models)

while the flood was apparently due to more local causes not include in the AGCMS. in contrast, the ENSO signals, as illustrated by maps of warm minus cool event averages, are generally similar between estimators, with an intriguing discrepancy between DAO and the models in the data-sparse central Indian Ocean. Finally, the water vapor flux and its potential influence upon the thermohaline circulation was examined and seen to be similar in both models and assimilation. These results suggest successful modeling of the global thermohaline circulation will need to include feedbacks between the circulation itself and meridional moisture flux(into the Ross Sea especially).

By intercomparing the ECHAM models and the DAO assimilation we have seen a number of consistent features that are typical of the atmosphere. Notable among these is the significant transport from tropics to higher latitudes in both hemispheres. Interestingly, the assimilations show considerably small-scale structure akin to jets of moisture that can also be seen in the models, e.g. the low level moisture jet over the United States. Thus the term 'tropospheric rivers' suggested by Newell and Zhu (1994) describes well the large time-average transport, but masks the high intermittence in both magnitude and direction, It is these features that feed both moisture and latent heat to midlatitude baroclinic eddies, and indeed are apparently closely coupled to them. One very notable feature of these midlatitude jets is their strong convergence, leading to only weak (but locally very important) transport into polar regions. This polar transport was noted above and seen to have a potentially important effect upon the global thermohaline circulation. in the tropics, strong jets of moisture move across the Pacific and converge in the regions of the Warm Pool, the Asian and Australian monsoons and the Amazon Basin. It is these tropical features that arc the dominant feature of the planet's water vapor transport (as manifested in the CEOFs discussed above). The tropical transport is modulated by the ENSO cycle, along with most other meteorological features of the tropics. Perhaps the most surprising result of our study, was that the features just noted appeared with roughly equal validity in both a reanalysis product that included nearly all available data and in a pair of AGCM runs forced only by observed global SST and the observed solar cycle

References:

Arakawa, A. and M.J.Suarez, 1983: Vertical differencing of the primitive equations in sigma coordinates. *Mon.Wea.Rev.*, *109,18-36.*

Barnett, T. P., 1983: Interaction of the Monsoon and Pacific Trade Wind systems at interannual time scales, Part 1, The equatorial zone, *Mon.Wea.Rev.*, **111** (4), 756-773.

Barnett, T. P., 1995: Monte Carlo climate forecasting. *J. Clim.*, 8(5), 1005-1022.

Bell, D. B. and J.E. Janowiak, 1995, Atmospheric Circulation Associated with the midwest floods of 1993, BAMS, 76 (5), 681-695,

Chahine, M. T., 1992: The hydrological cycle and its influence on climate, *Nature*, 359, 373-380.

Climate Diagnostics Bulletin, Available from Climate Analysis Center, NOAA, NOAA Science Center, Room 605, 5200 Auth Rd., Washington, DC 20233.

Gates, W. L., 1992: AMIP: The atmospheric model intercomparison project, *Bull. Am. Met. SO(',* 73(12), 1962-1970.

Gates, W. L., 1995: The validation of atmospheric models , Global Change. Luxembourg: Office for Official Publications of the European Communities, 218-232.

Hastenrath, S.1.., 1966: The flux of atmospheric water vapor over the Caribbean Sea and the Gulf of Mexico. *J. Appl.Met.*, *5,* 778-788.

Lau, W. K.-M, and Y.C. Sud, and J.-H. Kim, 1995: Intercomparison of Hydrological Processes in Global Climate Models, NASA I'ethnical Memorandum 104617, pp 1-161.

Matsuyama, H. 1992: The water budget in the Amazon River Basin during the FGGE period, J. *Met.* Sot. *Japan*, 70(6), 1071-1083.

Mo, K.C, J. Nogues-Paegle, and J. Paegle, 1995, Physical mechanisms of the 1993 summer floods, *J. Afro. Ski.,* 52 (7), 879-895.

Mo> K.C., and W. Higgins, 1996, Large-scale atmospheric transport as evaluated in the NCEP/NCAR and the NASA/DAO Reanalysis, 1996. Submitted to *J. Clim.*

Molod, A., H.M. Helfand, and L.L. Takacs, 1996: The climate of the GEOS-1 GCM and its impact on the GEOS- 1 data assimilation system. Submitted.

North, G. R., T.L. Bell, R. F'. Cahalan, and F.J. Moeng, 1982: Sampling Errors in the Estimation of Empirical Orthogonal Functions. *Mon.Wea.Rev.*, **110,** 699-706

Newell, R.E. and Y. Zhu, 1994: Tropospheric rivers: A one-year record and a possible application to ice core data. *Geophys.Res.Let.*, 21 (2), 113-116.

Osbom, T, J., 1995: Internally-generated variability in some ocean models on decadal to millenial time scales. Ph.D. Thesis, Climatic Research Unit, School of Environmental Sciences, University of East Anglia, U.K.

Peixoto, J.I'., D.A. Salstein, and R.D. Rosen, 1981: Intra-annual variation in large-scale moisture fields. *J. Geophys. Res.*, **86(C2), 1255-1264.**

Peixoto, J.P. and A.H. Oort, 1983: The atmospheric branch of the hydrological cycle and climate. In: *Variations in the Global Water Budget, D.* find Publishing Company, pp. 5-65.

Pfaendtner, J., S. Bloom, D. Lamich, M. Seablom, M. Sienkiewicz, J. Stobie, and A. da Silva, 1995: Documentation of the Goddard Earth Observing System (GEOS) Data Assimilation System - Version I. NASA Technical Memo 104606, Vol. 4,44 pp.

Pierce, D.W., T.P. Barnett, and U. Mikolajewicz, 1995: On the competing roles of heat and fresh water flux in forcing thermohaline oscillations. *J. Phys. Oceanogr., 25(9), 2046-2064.*

Prcisendorfer, R. W. and T. P. Barnett, 1983: Numerical model-reality intercomparison tests using small-sample statistics. *J. Atm. Sci.,* **40(8), 1884-1896.**

Roads, J. O., S.C. Chen, A.K. Guetter, and K.P. Georgakakos, 1994: Large-scale aspects of the United States hydrologic cycle. Bull. Am. Met. Sot., 75(9), 1589-1610.

Roeckner, E., K. Arpe, I.. Bengtsson, S. Brinkop, L. Dumenil, M. Esch, E. Kirk, F. Lunkcit, M. Ponatcr, B. Rockel, R. Sausen, U. Schlese, S. Schubert, and M. Windelband, 1992: Simulation of the present-day climate with the ECHAM model: Impact of model physics and resolution. Max Planck Institut fur Meteorologic, Rep. No. 93, October, 1992, 171 pp"

Rasmussen, E. M., 1966: Diurnal variations in the summer water vapor transport over North America, *Water Resources Res.*, 2(3), 469-477.

Rasmussen. E.M., 1967: Atmospheric water vapor transport and the water balance of North America: Part 1. Characteristics of the water vapor flux field *Mon. Wea. Rev.,* 9 5(7), 403-426.

Rasmussen, E. M., 1968: Atmospheric water vapor transport and the water balance of North America: Part II. Large-scale water balance investigations. *Mon. Wea. Rev.,* **96(10), 720-734.**

Rosen, R. D., D.A. Salstein, and J. F'. Peixoto, 1979: Variability in the annual fields of large-scale atmospheric water vapor transport. *Mon. Wea. Rev., 107,* 26-37.

Schubert S. D., J. pfaendtner, and R. Rood, 1993: An assimilated data set for Earth Science Applications. *Bull. Am. Met. Sot.,* 74, 2331-2342.

Starr, V.P. and J.P. Pcixoto, 1958: On the global balance of water vapor and the hydrology of deserts. *Tellus, 10,* 189-194.

Suarez, M.J. and L.L. Takacs, 1995: Documentation of the Aries-GEOS Dynamical Core: Version 2. NASA Technical Memo 104606, Vol. 5. .

Takacs, 1..1/., A. Molod, and T. Wang, 1994: Documentation of the Goddard Earth Observing System (GEOS) Data Assimilation System - Version 1. NASA Technical Memo 104606, vol. 1, 100 pp.

Tiedtke, M., 1989: A comprehensive mass flux scheme for cumulus parametrization in large-scale models. *Mon.Wea.Rev.*, **11** 7, 1779-1800.

Tiedtke, M., W.A. Neckley, and J. Slingo, 1988: Tropical forecasting at ECMWF: On the influence of physical parametrization on the mean structure of forecasts and analyses. *Quart. J. Rov. Met, Sot.,* **114**, 639-664.

Trenberth, K.E. and G.W. Branstator, 1992: issues in establishing causes of the 1988 drought over North America. *J. Clim.*, S(2), 159-172

Wang, M. and J. Paegle, 1996: Impact of analysis uncertainty upon regional atmospheric moisture flux, *J. Geophys. Res.*, in press.

Williamson, D.L. and P.J. Rasch, 1994: Water vapor transport in the NCAR-CCM2. *Tellus*, 46A, 34-51.

Table Captions:

Table 1. Locations of radiosonde stations used in this study.

Table 2. Biases of DAO and ECHAM4 flux fields, as percentage difference between the magnitude of the time average fluxes and associated radiosonde quantity. The geographical regions arc chosen by station clusters in figure 3.

Figure Captions:

Figure 1. Correlation between time series of radiosonde and a) DAO and b) ECHAM4 water vapor flux for the period March 1985 to February 1990, versus boxcar filter width, for Dodge City.

Figure 2. Same as figure 1, but for Curacao.

Figure 3. Map of correlation between series of radiosonde and DAO Q-fluxes at the stations listed in table 1, over the period March 1985 to February 1990. Arrow lengths are proportional to correlation magnitude. Correlation phase of zero points to the east and, 90 degrees to the north.

Figure 4. Map of correlation between series of radiosondc and DAO Q-fluxes as in figure 3, but after smoothing the input series with a 400 day width boxcar function.

Figure 5. Radiosonde-ECHAM4 correlation, same processing as in figure 4.

Figure 6. Five year average (March 1985-February 1990) vertically integrated water vapor flux in a) the DAO assimilations, b) the ECHAM3 model. and, c) the ECHAM4 model. An arrow of magnitude 400 kg / (m-s) is shown for reference. Notice the general similarity between the three plots.

Figure 7. Zonal mean zonal water vapor flux from each of the three fields depicted in figure 6. plus estimates from Piexoto and Oort (1983). The two AGCMs and the DAO agree to about 10'!4 while the radiosonde-based estimates differ by as much as 75°/0 in the data sparse Southern I hemisphere.

Figure 8. Difference between five year average DAO flux depicted in figure 6a and, a) averaged ECHAM3 flux depicted in figure 6b, and, b) averaged ECHAM4 depicted in figure 6c. An arrow of magnitude 150 kg / (m-s) is shown for reference. Onc interesting feature is the similarity between ECHAM3 and ECHAM4, an unexpected result given the dramatic change in moisture transport mechanisms between the two models.

Figure 9. Zonal mean zonal water vapor flux averaged over the years 1985-1990 and the months of a) June, July and August, and, b) December, January and February, for each of the DAO, ECHAM3 and ECHAM4 fields, plus comparable estimates from Piexoto and Oort (1983). The largest discrepancies between AGCMs occur in JJA in the midlatitudes.

Figure 10. Water vapor flux averaged over the months of December, January and February, 1985-1990 for a) DAO, b) ECHAM4 fields. Good general agreement between the fields with ECHAM4 showing the larger transport in the tropics.

Figure 11. Water vapor flux averaged over the months of June, July and August and the years 1985-1990 for a) DAO, b) ECHAM4 fields.

Figure **12, EOFs of the Moisture Flux for 5 years** of DAO, ECHAM3, ECHAM4 data. The EOFs were applied to 30 day averaged values and the grand mean was subtracted from each. The figure is dominated by the Asian monsoon signature.

Figure 13. Time series of a) the amplitude of the first complex EOF in the monthly averaged DA() water vapor flux fields, over the period March-1985-February 1990. Also shown are a) the magnitudes of the projections of this EOF onto the similarly averaged ECHAM3 and ECHAM4 water vapor fluxes, and, b) associated phases.

Figure 14. a) DAO and. b) ECI IAM4 moisture anomaly for May/June 1988 over the US. DAO shows a larger anomaly over the southern gulf states and the position the Bermuda High.

Figure 15. a) DAO and, b) ECHAM4 moisture flux amplitude for June/July 1993 over the US. DAO agrees well with other data sources in the approximate location of the maximum amplitude of the moisture flux. ECHAM4, as might be expected because of the more local nature of this event, misses the flood conditions.

Figure 16. Water vapor flux averaged over the period December 1989-February 1990 minus the average over December 1987-February 1988 for a) DAO, and, b) ECHAM4. Both models capture the significant features of the EN SO event.

Figure 17. The 5 year averaged U-Flux at 60S is presented in the upper panel for the three models, DAO, ECHAM3 and ECHAM 4. The bottom panel is the 5 year averaged V-Flux. The Ross Sea is about 150W.

Figure 18 Moisture flux as a function of time through a rectangular box (60 S-75S, 135E-165E). Starting at the upper left corner, the flux through the left boundary, right, bottom, and top. Almost all of the transport comes from the northern boundary, i.e. across 60S.

Figure 19. Total moisture flux (E-P) as a function of time through a rectangular box (60 S-75S, 135E-165E). This figure shows the region is usually receiving water from the north and precipitation exceeds local evaporation.

TABLE 1

Station No.	Station Name	Longitude	Latitude
116410b	San Juan	66.00 w	18.26 N
116430b	Curacao	68,58 W	12.12 N
116450b	St. Martin	63.07 W	18.03 N
117060b	Guantanamo Bay	75.09 w	19.54 N
117150b	Kingston	76.47 W	17.56 N
118130b	Grand Cayman	81.22 W	19.18 N
119040b	Vera Cruz	96.07 W	19.09 N
128500b	Key West	81.47 W	24.35 N
128780b	Merida	89.41 W	20.57 N
139850b	Dodge City	99.58 W	37.46 N
145030b	Stephenville.	58.33 W	48.32 N
146420b	Sable Island	60.01 W	43.56 N
215040b	Hilo	155.04 w	19,43 N
220090b	Mazatlan	106.25 W	23.11 N
225360b	Lihue	159,21 W	21.59 N
227010b	Midway Is..	177.23 W	28.12 N
255010b	Kodiak	152.20 W	57.45 N
255030b	King Salmon	156.39 W	58.41 N
256240b	Cold Bay	162.43 W	55.12 N
257040b	Atak	176.38 W	51.53 N
257130b	St. Paul Is..	170.13 w	57.09 N
31310b	San Diego	117,08 W	32.49 N
38810b	Centerville	87.15 W	32.54 N
39370b	Lake Charles	93.13 w	30.07 N
39400b	Jackson	90.05 w	32.19 N
39510b	Longview	94.39 w	32.21 N
403080b	Yap	138.05 E	9.29 N
407100b	Majuro	171.23 E	7.05 N
414150b	Guam	144.50 E	13.33 N
416060b	Wake Is.	166.39 E	19.17 N
517010b	Lima, Peru	77.08 W	12.01 s
617050b	Pago-Pago	170.43 w	14.20 S
684240w	Upington	21.16 E	28.24 S
684420w	Bloemfontein	26.18 E	29.06 S
685880w	Durban	30.57 E	29,58 S
688160w	Cape Town	18.36 E	33,58 S
688420w	Port Elizabeth	25.36 E	33,59 s
689940w	Marion Island	37.52 E	46.53 S

TABLE 2

Geographic Region	Number of Stations	DAO Bias Range (percent)	ECHAM4 Bias Range (percent)	Possible causes for largest biases In region
Far North Pacific	5	-22 to 61	27 to 301	Land-sea contrasts.
Central Pacific	3	-30 to 32	78 to 271	Island sea breeze effects.
Western Pacific	4	-28 to O	-60 to 9	
Southest U. S. A.	5	-33 to -21	-30 to 20	Strong Humidity gradients.
Caribbean	9	-36 to 17	-46 to 35	Strong gradients, island effects.
South Africa	5	-19 to 39	-34 to 85	Strong gradients, topographic effects.

Fig. 1a

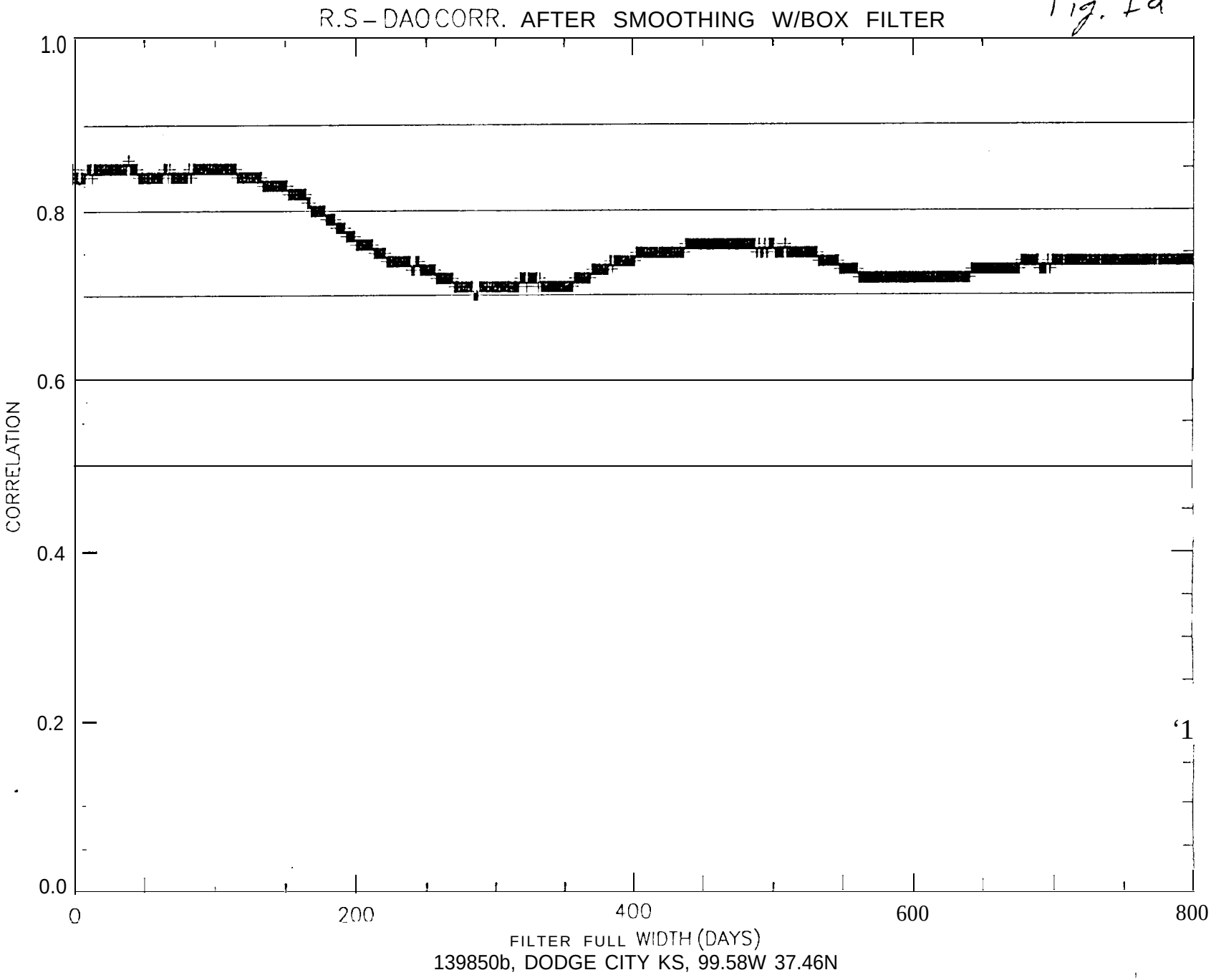
R.S – DAO CORR. AFTER SMOOTHING W/BOX FILTER
1.0
0.8
0.6
0.4
0.2
0.0
CORRELATION
0
200
400
600
800
FILTER FULL WIDTH (DAYS)
139850b, DODGE CITY KS, 99.58W 37.46N

Box

R.S – EC4 CORR. AFTER SMOOTHING W/~~TRIANGULAR~~ FILTER

Fig. 15

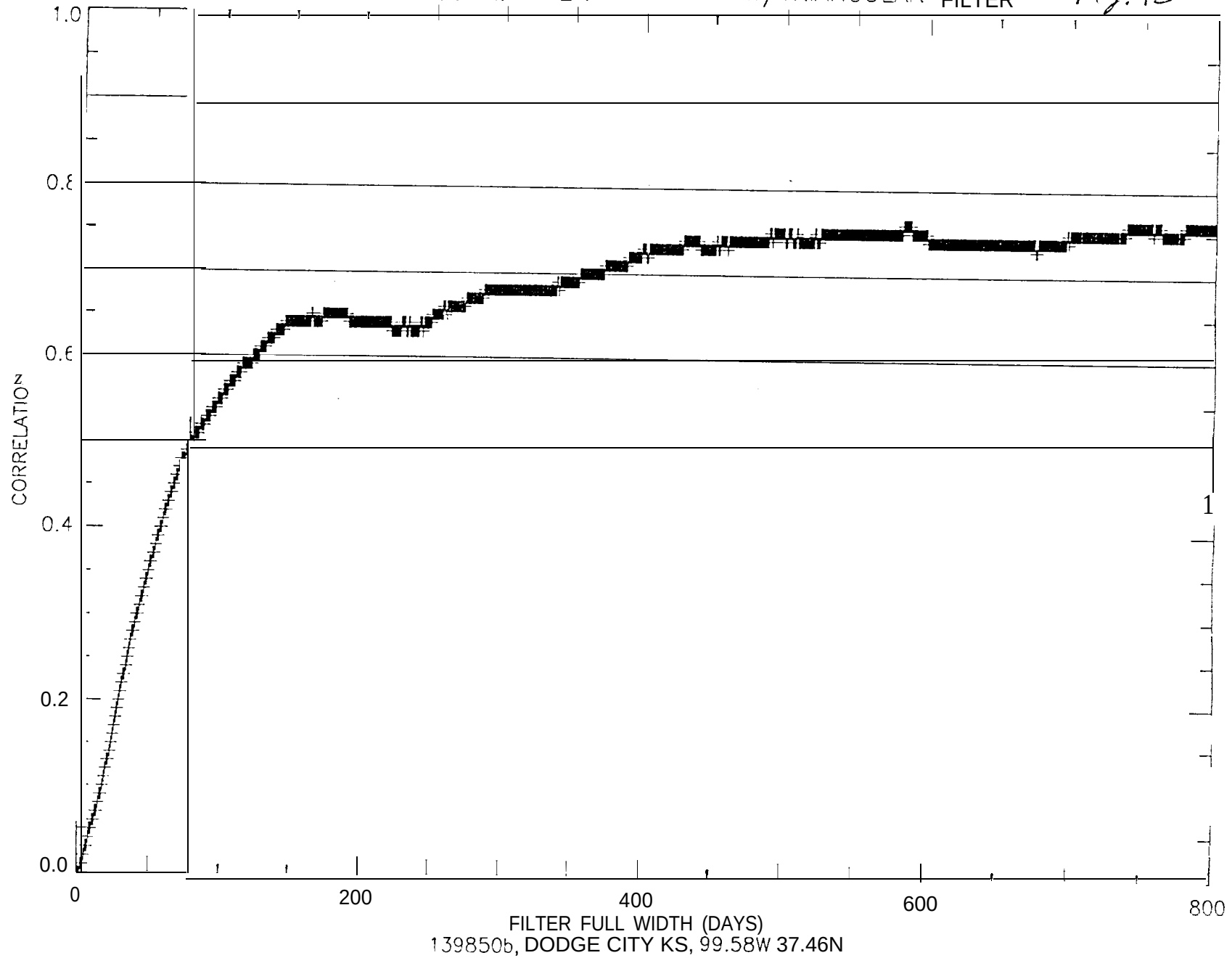

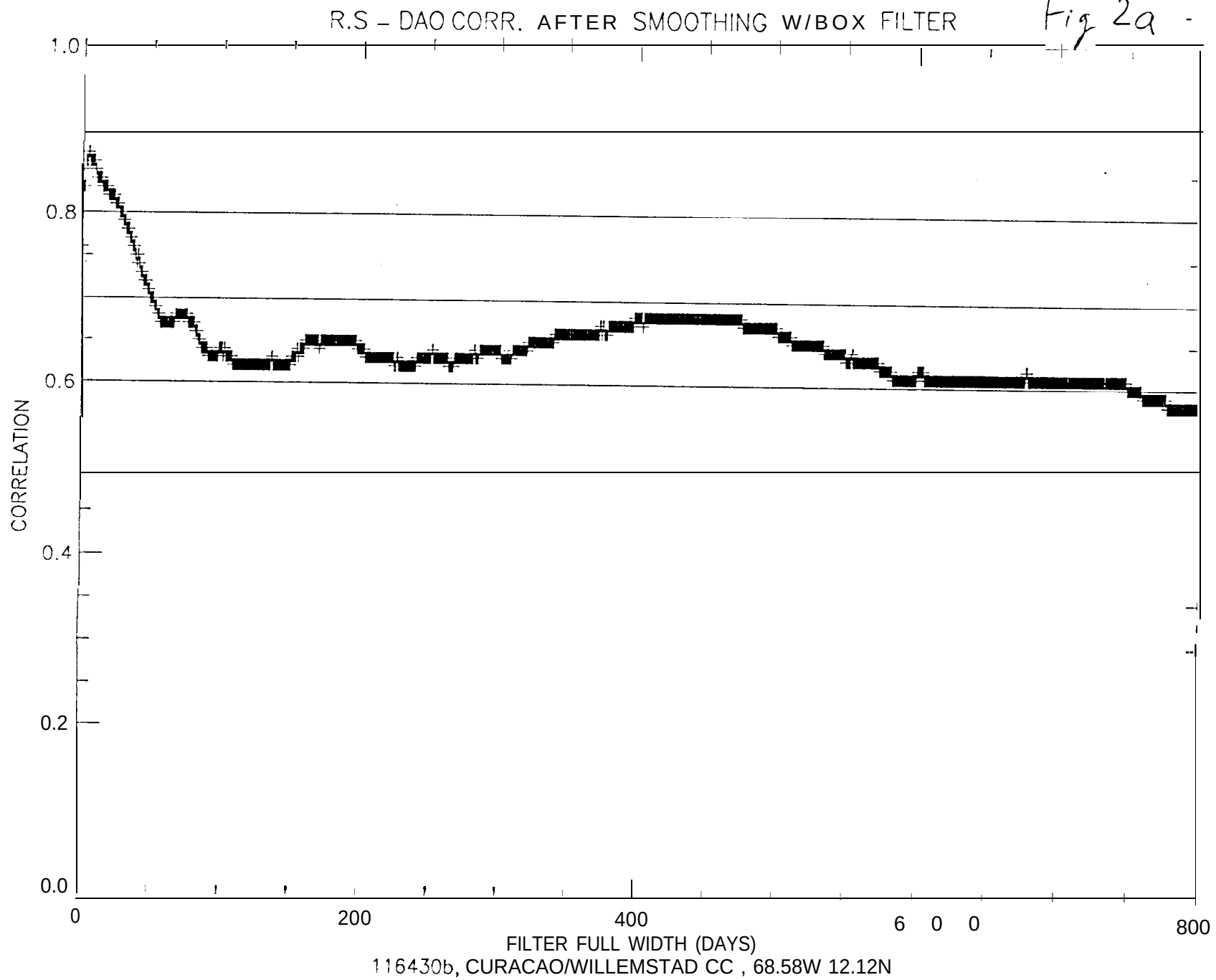
R.S – DAO CORR. AFTER SMOOTHING W/BOX FILTER
Fig 2a
1.0
0.8
0.6
0.4
0.2
0.0
CORRELATION
0
200
400
600
800
FILTER FULL WIDTH (DAYS)
116430b, CURACAO/WILLEMSTAD CC , 68.58W 12.12N

BOX

R E — EC4 CORR AFTER SMOOTHING w/~~TRIANGULAR~~ FILTER

Fig 2L

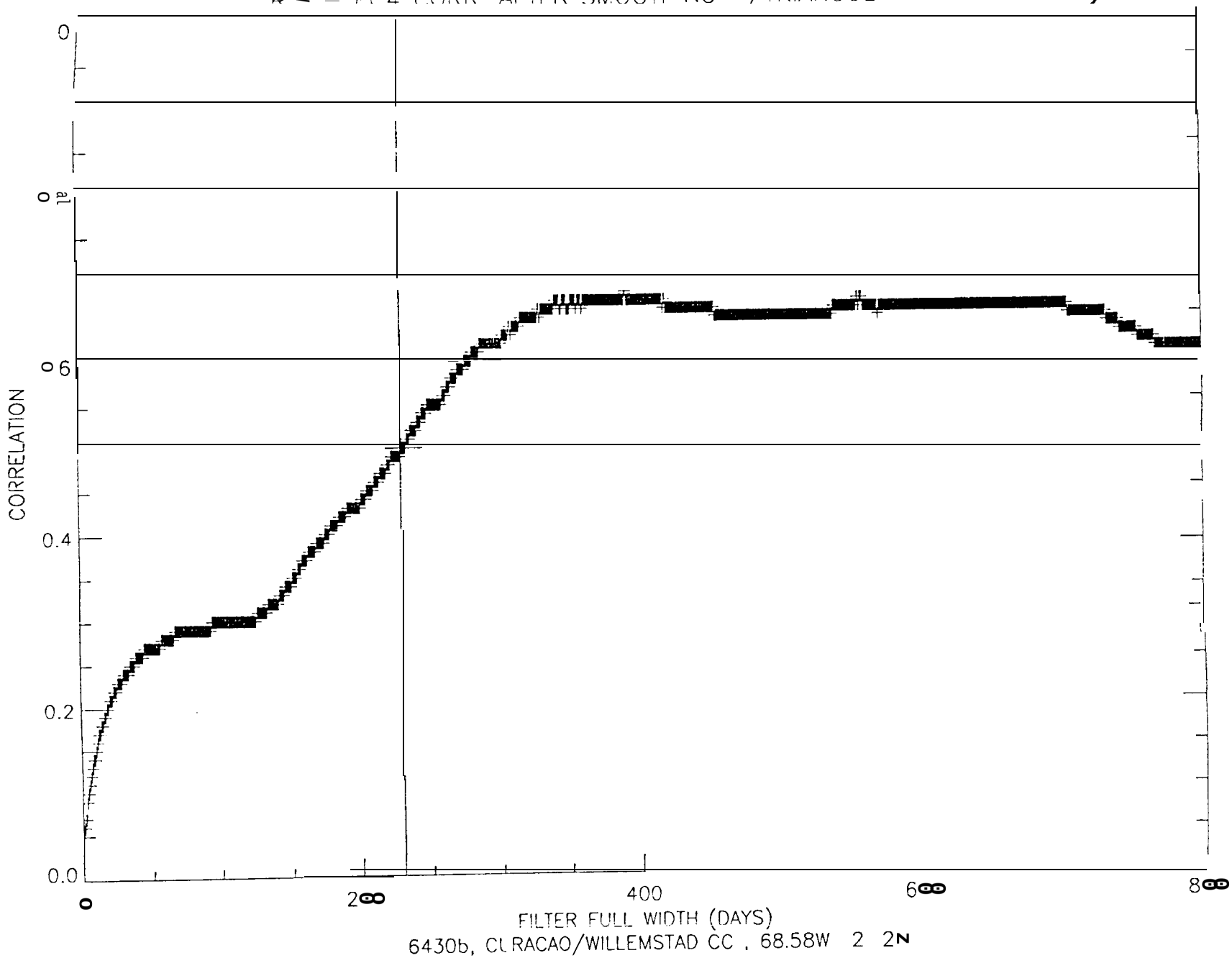

Fig. 3

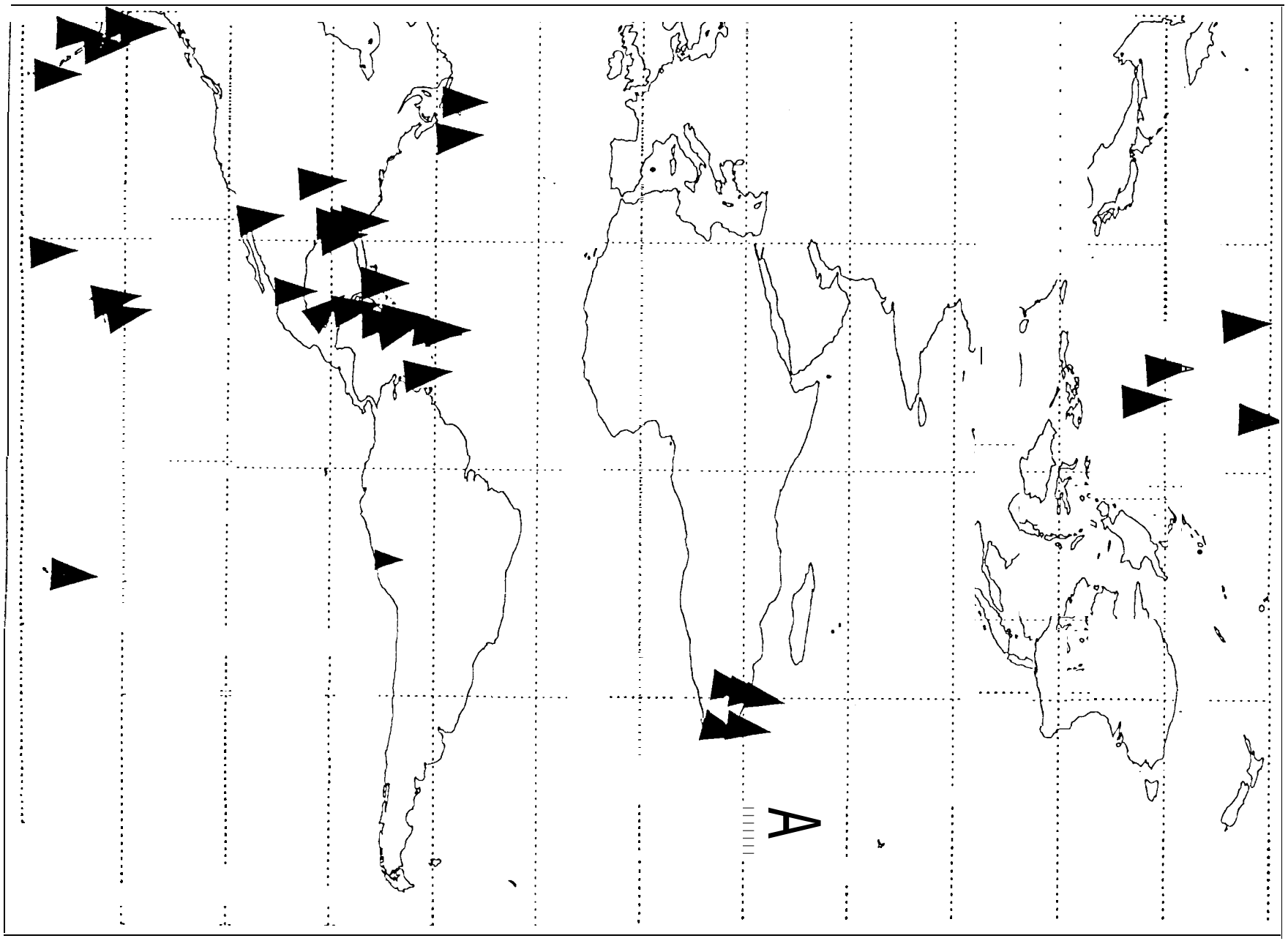

Fig 4

DAO–400 DAY BOX FILTER

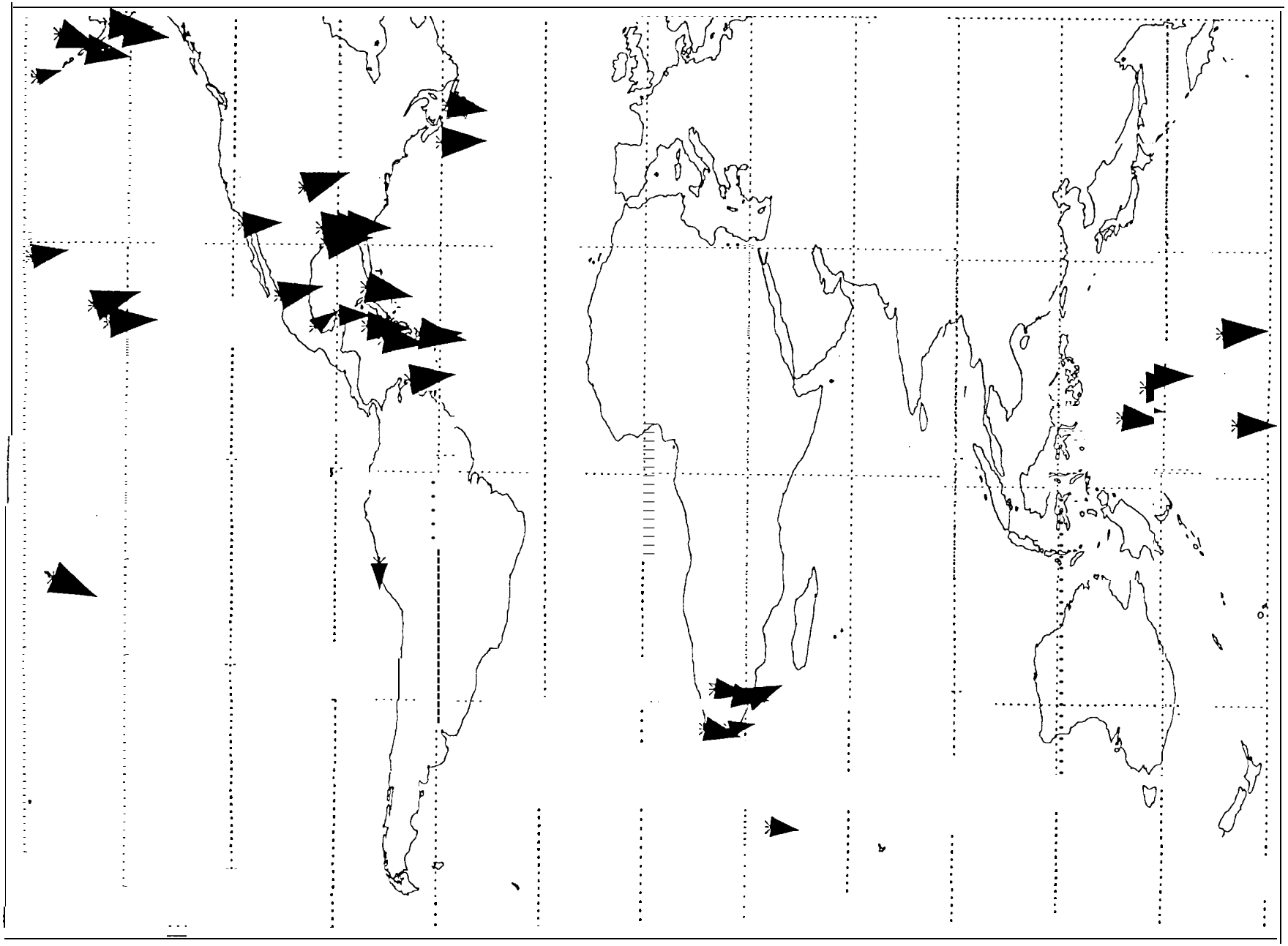

Fig. 5

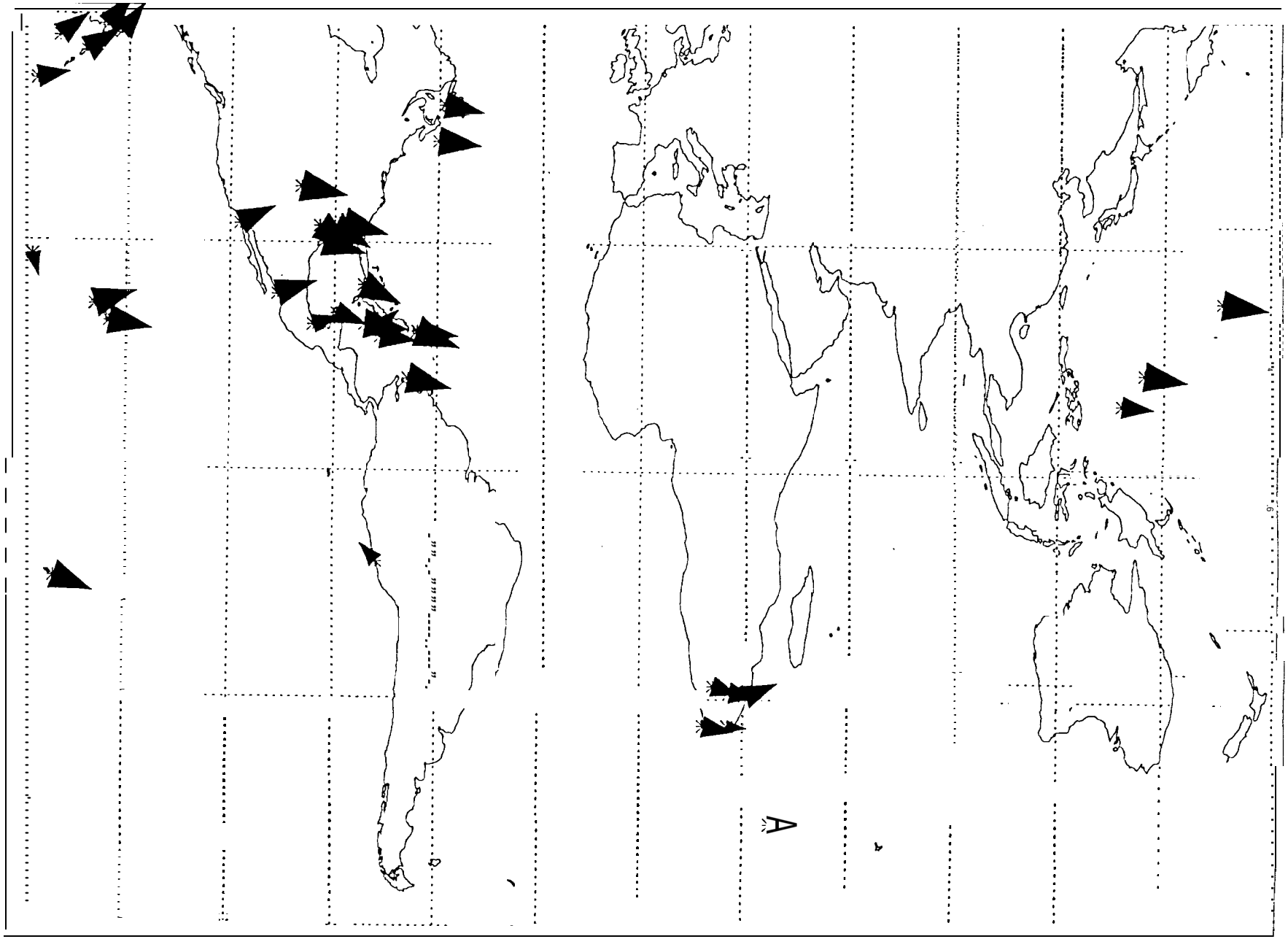

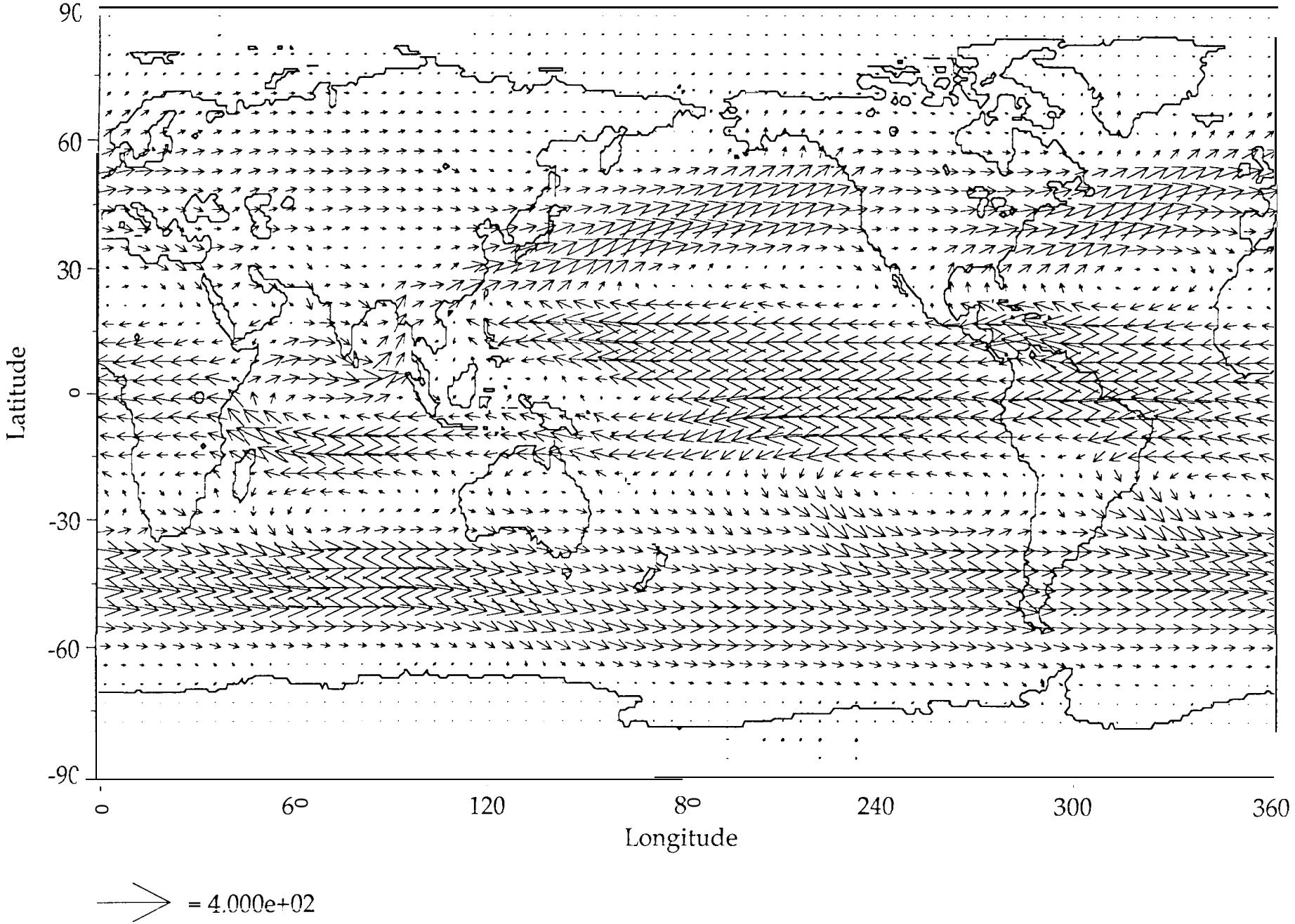
90
60
30
0
-30
-60
-90
Latitude
0
60
120
80
240
300
360
Longitude
= 4.000e+02

Fig 6a

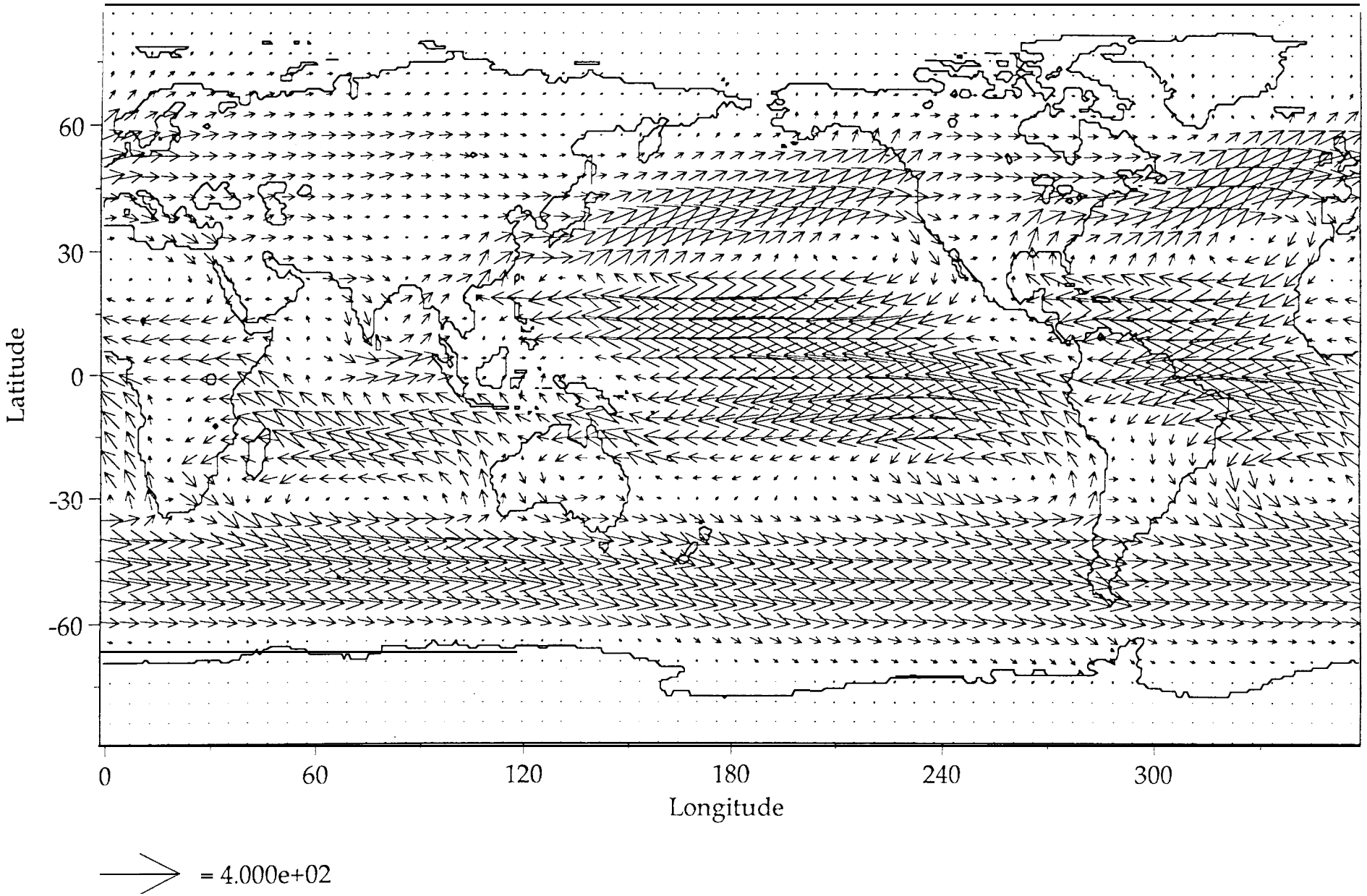

Fig 6b

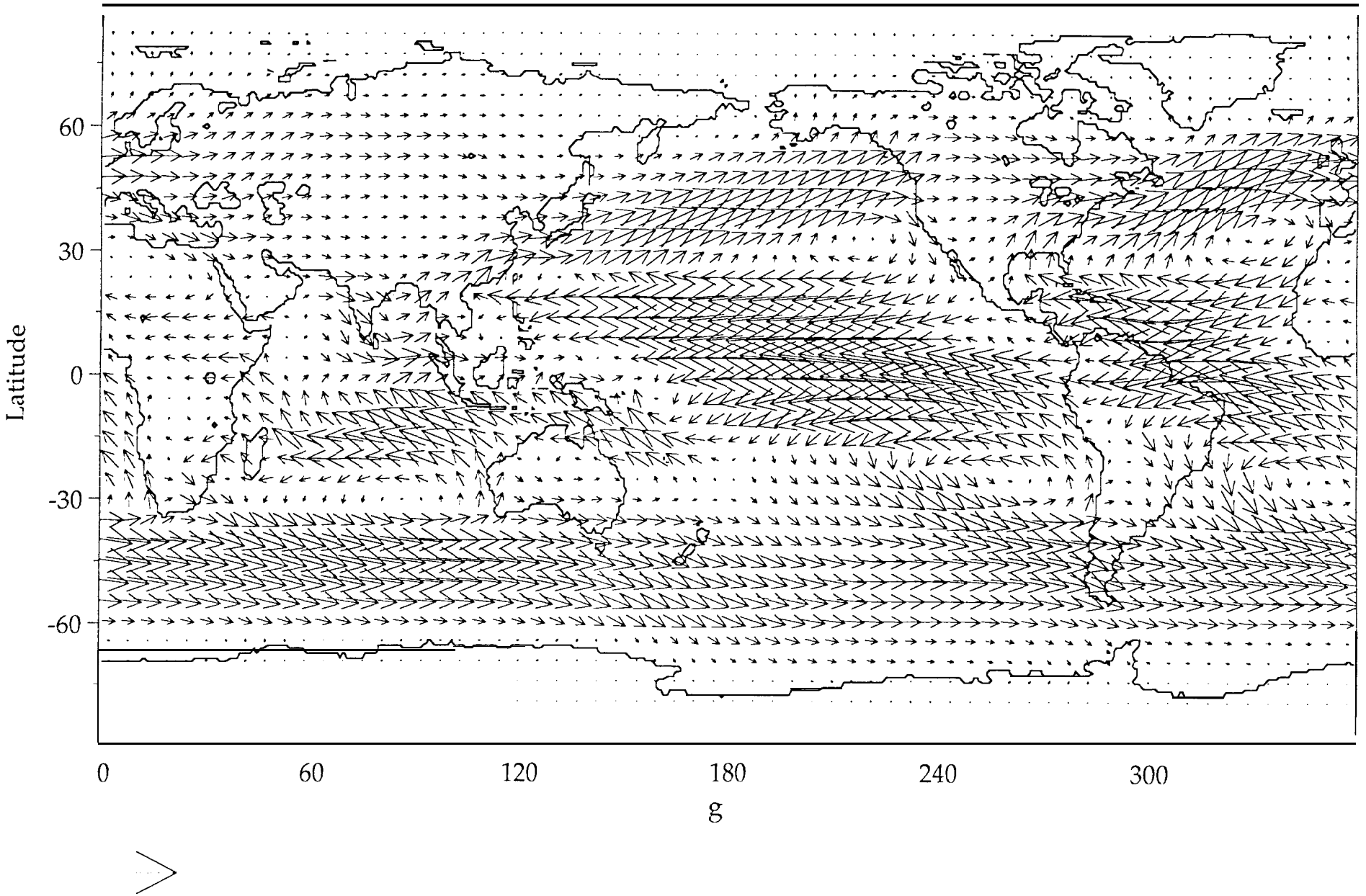
60
30
0
-30
-60
Latitude
0
60
120
180
240
300
g

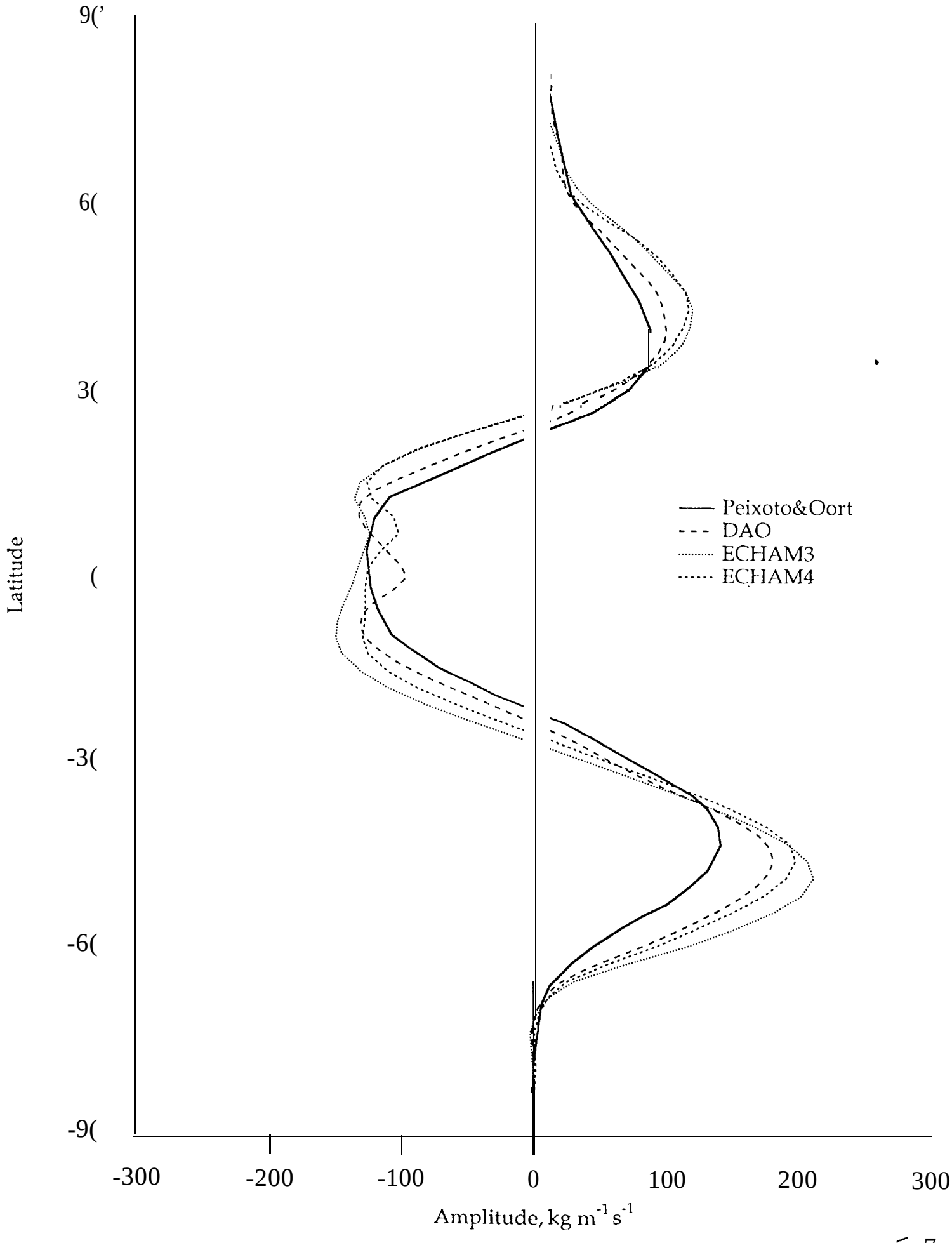
9(’
6(
3(
(
-3(
-6(
-9(
Latitude
-300
-200
-100
0
100
200
300
Amplitude, kg m-1 s-1
Peixoto&Oort
DAO
ECHAM3
ECHAM4

Fig 7

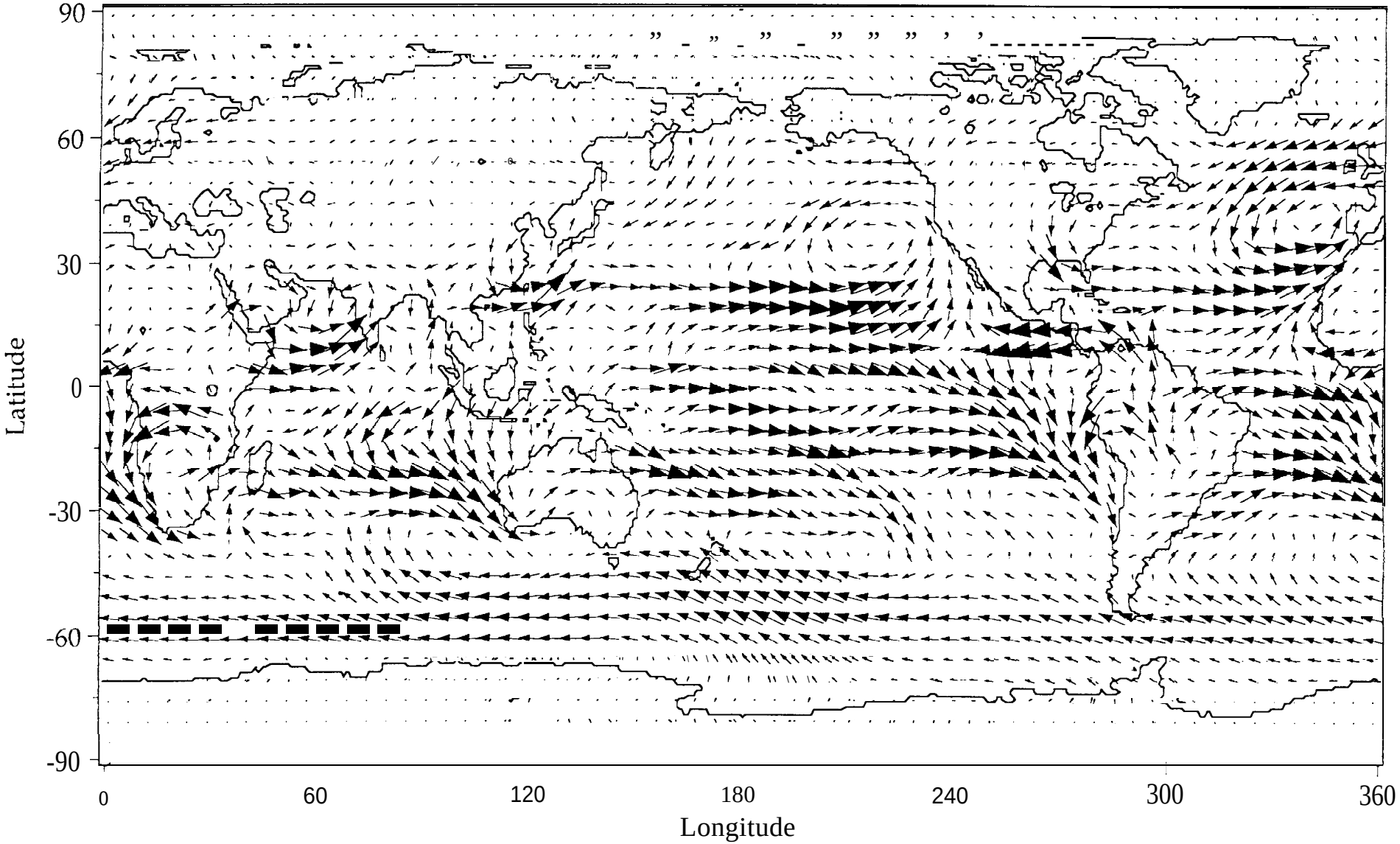
90
60
30
0
-30
-60
-90
Latitude
0
60
120
180
240
300
360
Longitude
= 1.500e+02

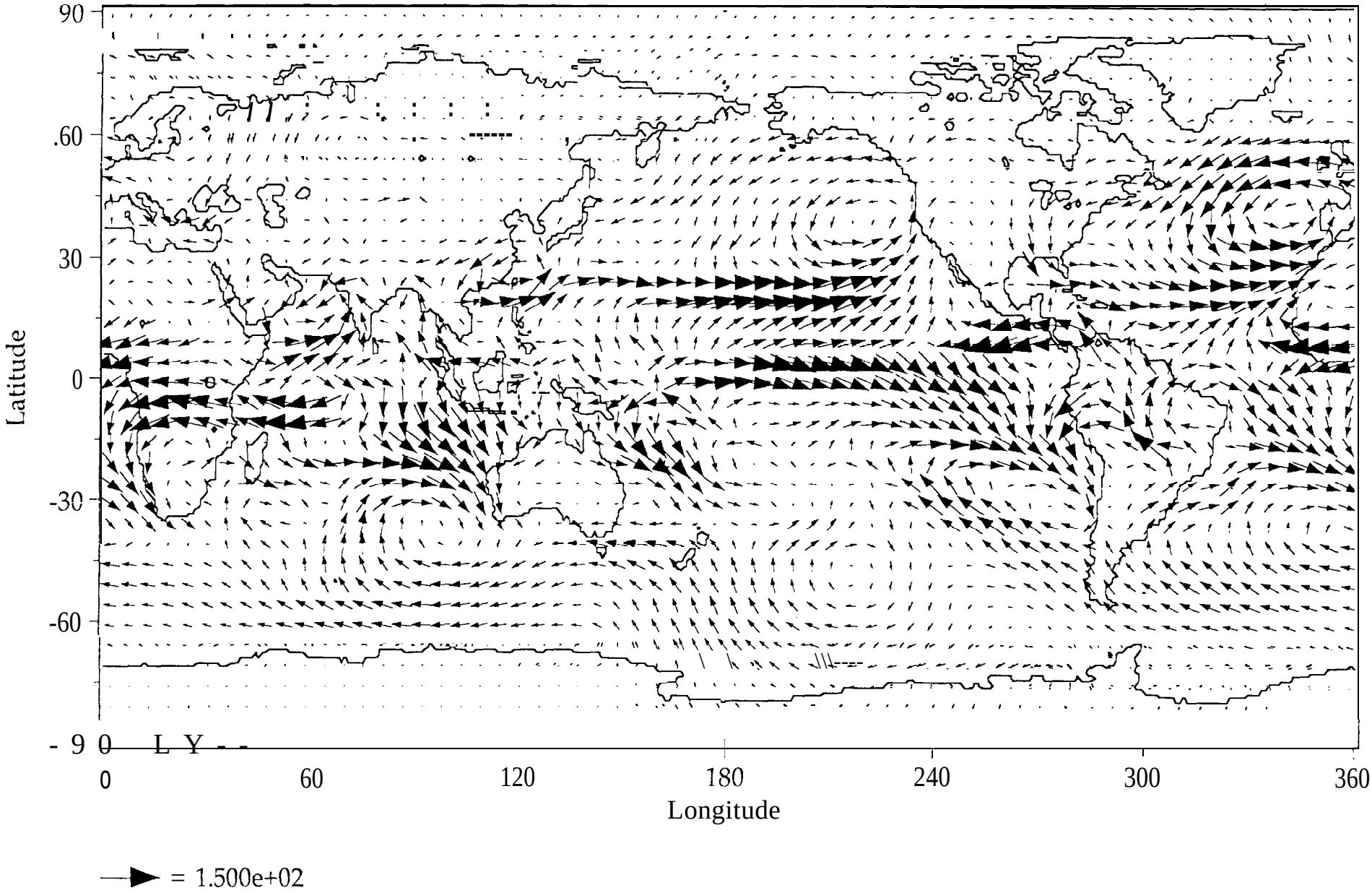
90
.60
30
0
-30
-60
- 9 0
Latitude
0
60
120
180
240
300
360
Longitude
= 1.500e+02

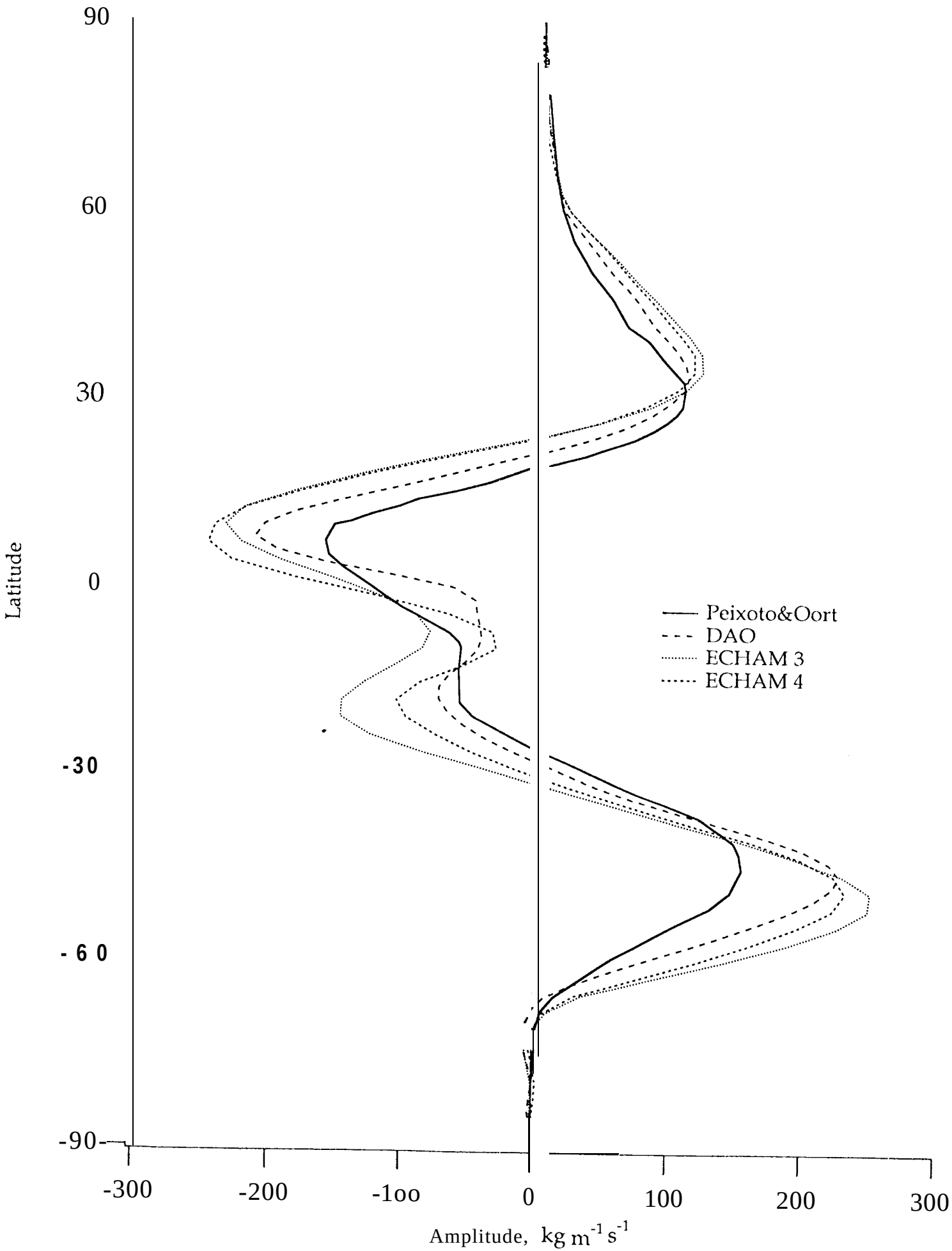
90
60
30
0
-30
-60
-90
Latitude
-300
-200
-1oo
0
100
200
300
Amplitude, kg m-1 s-1
Peixoto&Oort
DAO
ECHAM 3
ECHAM 4

Fig 9a

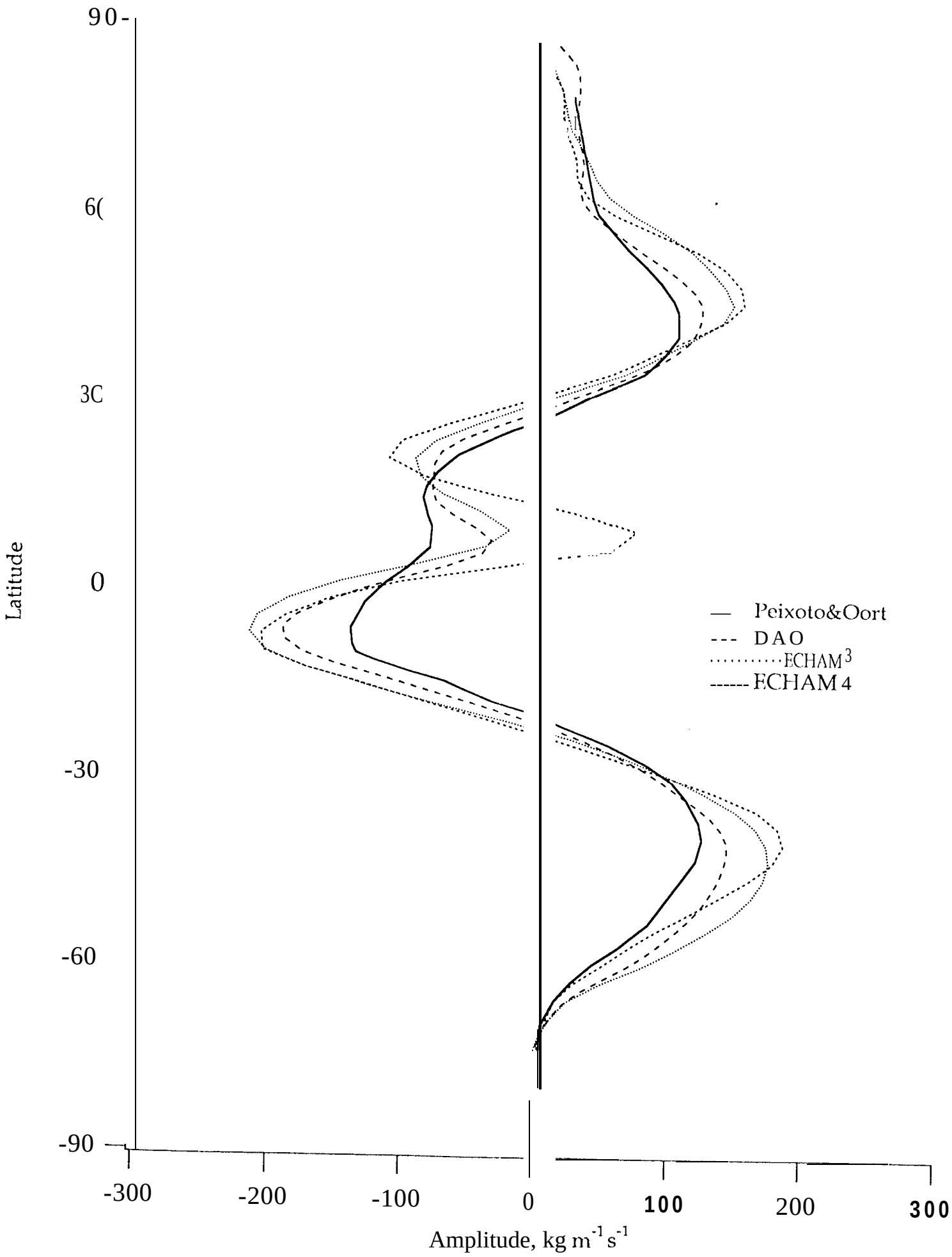
90
6(
3C
0
-30
-60
-90
Latitude
-300
-200
-100
0
100
200
300
Amplitude, kg m-1 s-1
Peixoto&Oort
DAO
ECHAM3
ECHAM4

Fig 9b

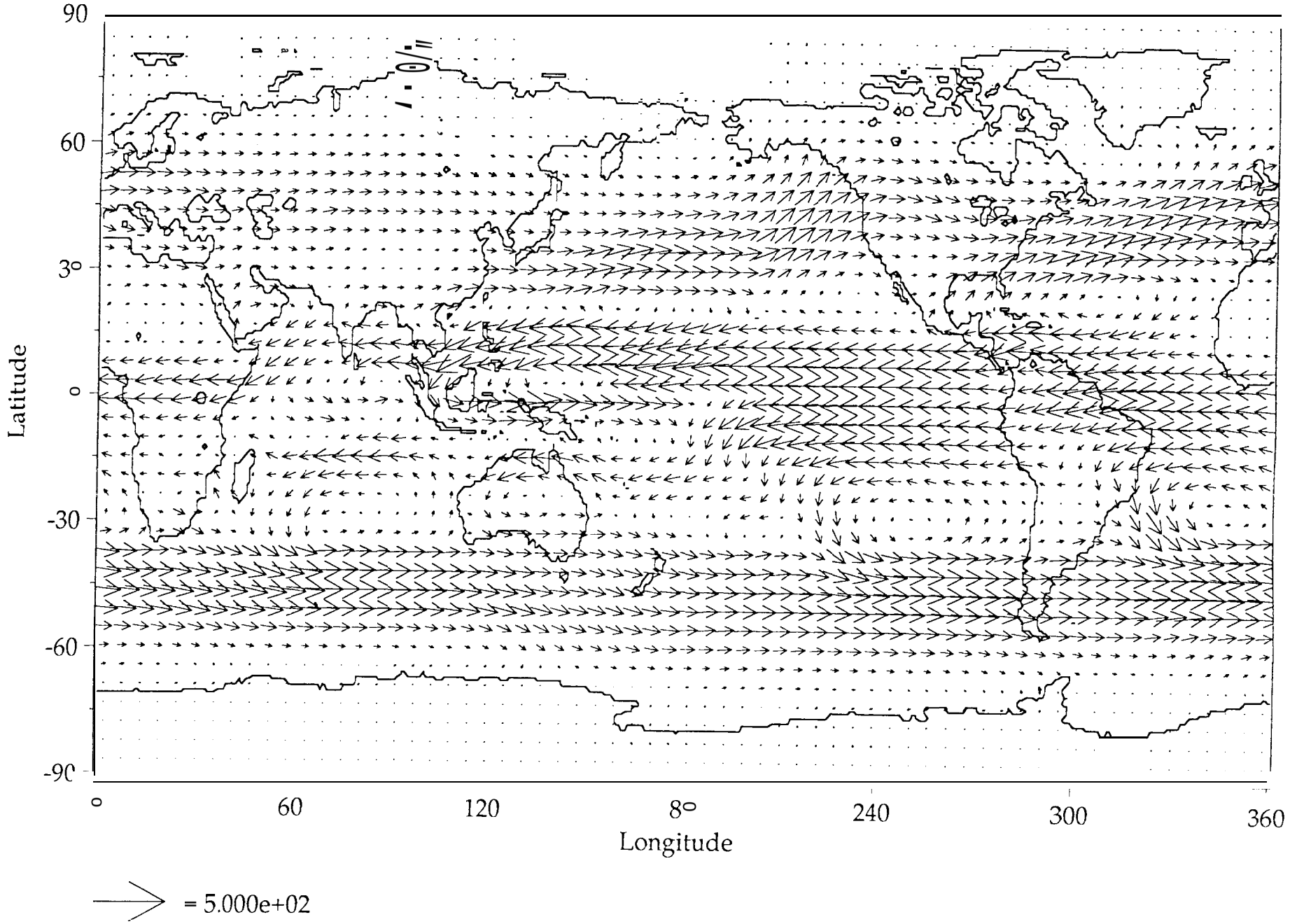
90
60
3o
0
-30
-60
-90
Latitude
0
60
120
8o
240
300
360
Longitude
= 5.000e+02

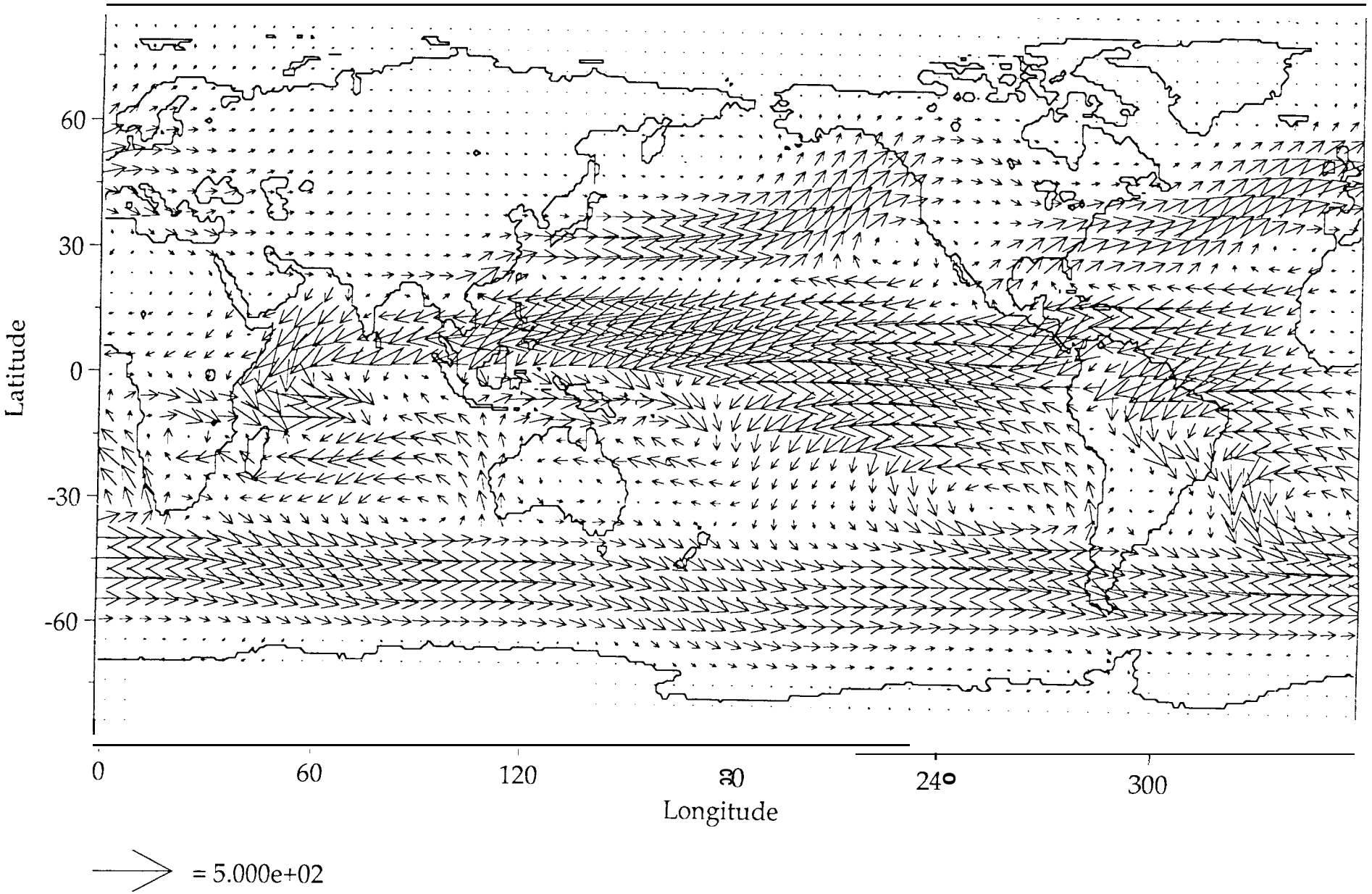
60
30
0
-30
-60
Latitude
0
60
120
180
240
300
Longitude
= 5.000e+02

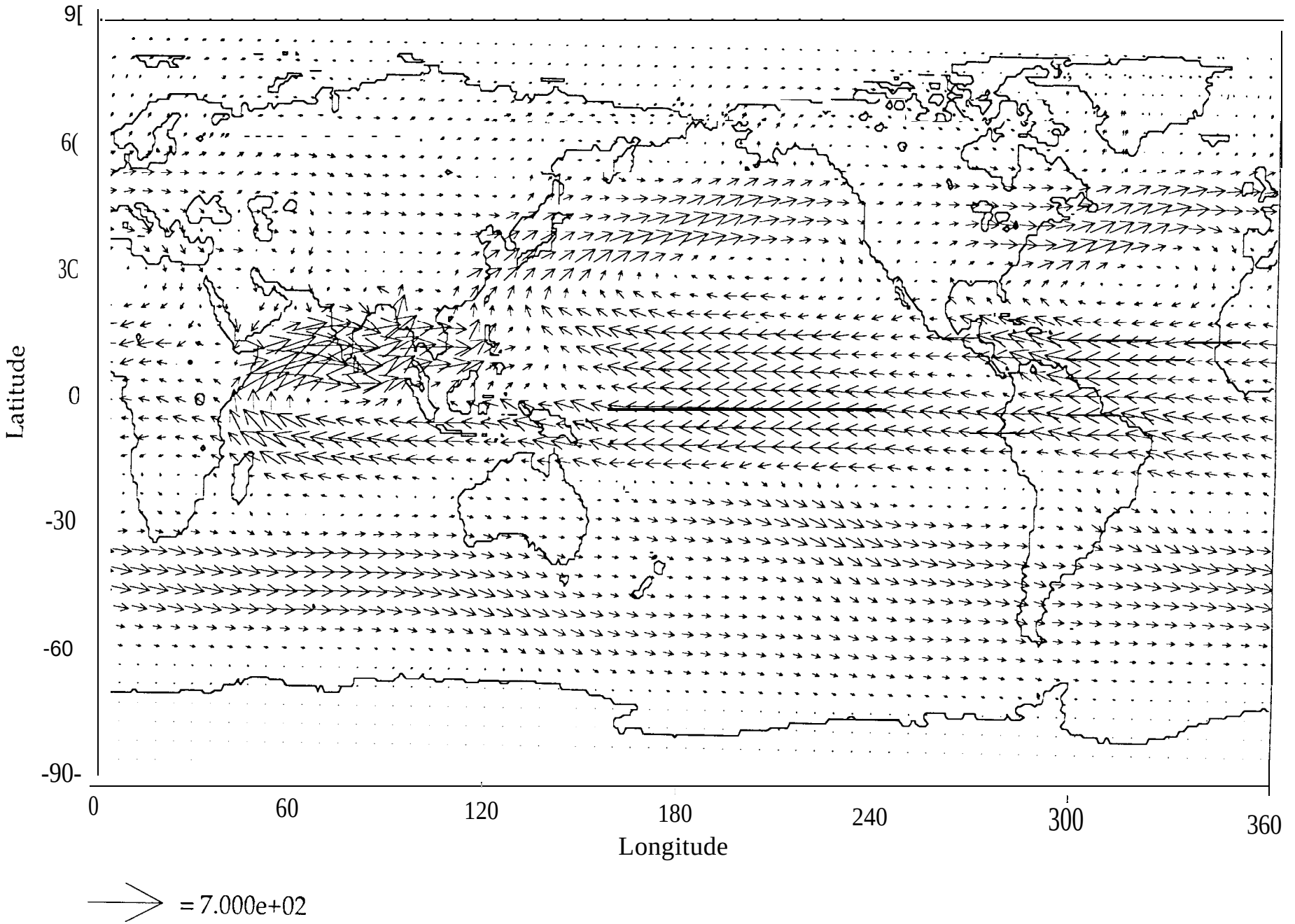
9[
6(
3C
0
-30
-60
-90-
Latitude
0
60
120
180
240
300
360
Longitude
= 7.000e+02

Fig 11a

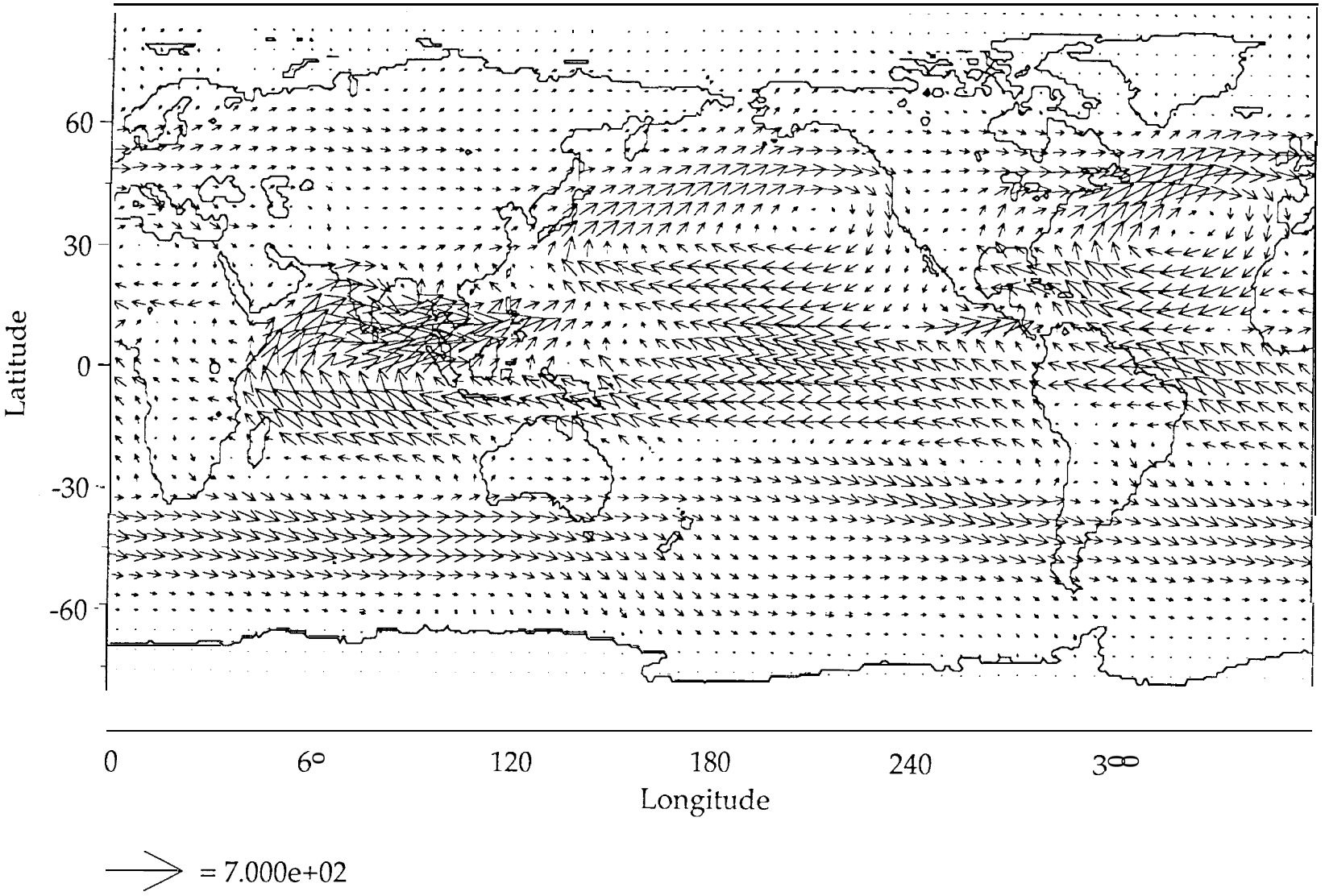
60
30
0
-30
-60
Latitude
0
6°
120
180
240
3∞
Longitude
= 7.000e+02

Moisture Flux Grand Mean Subtracted 5 yr/30 clay average (EOF1)

DAO

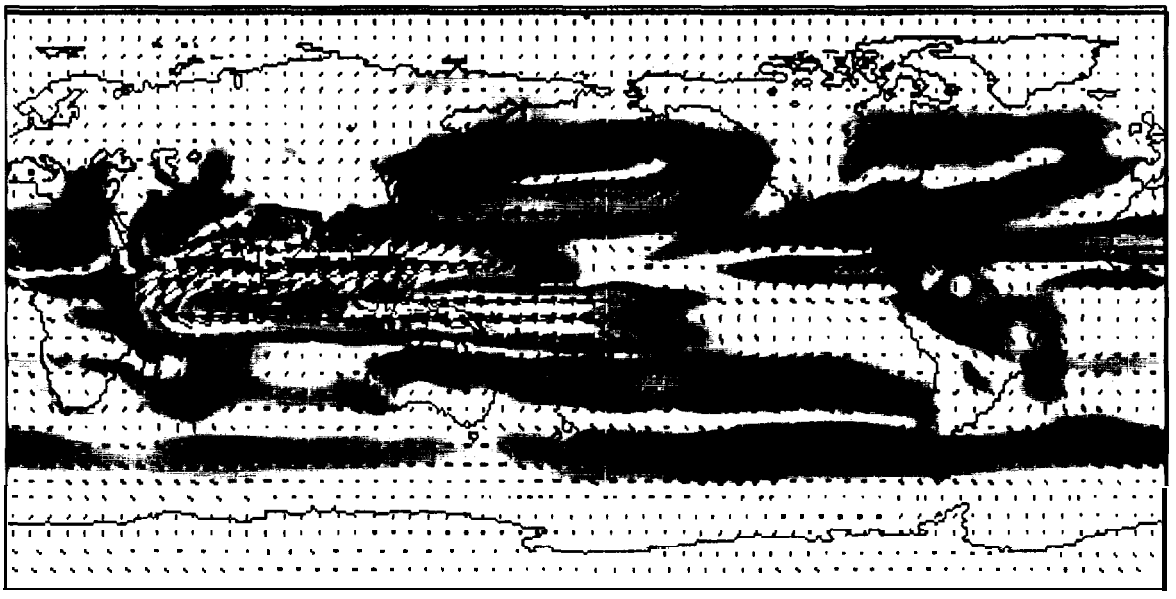

ECHAM3

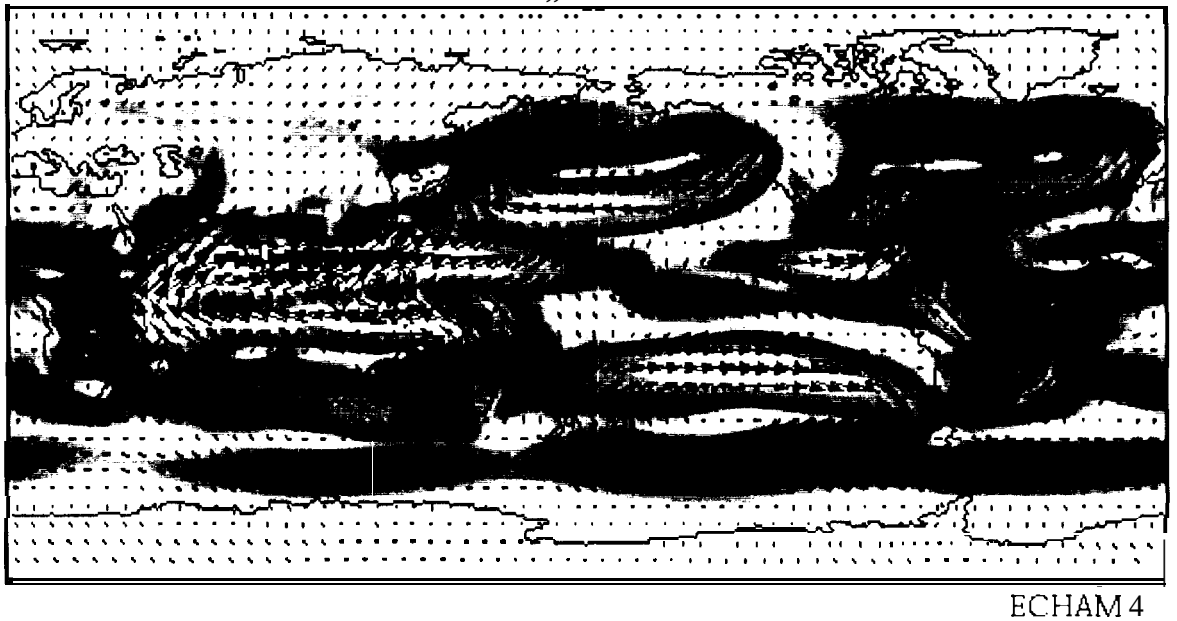

ECHAM 4

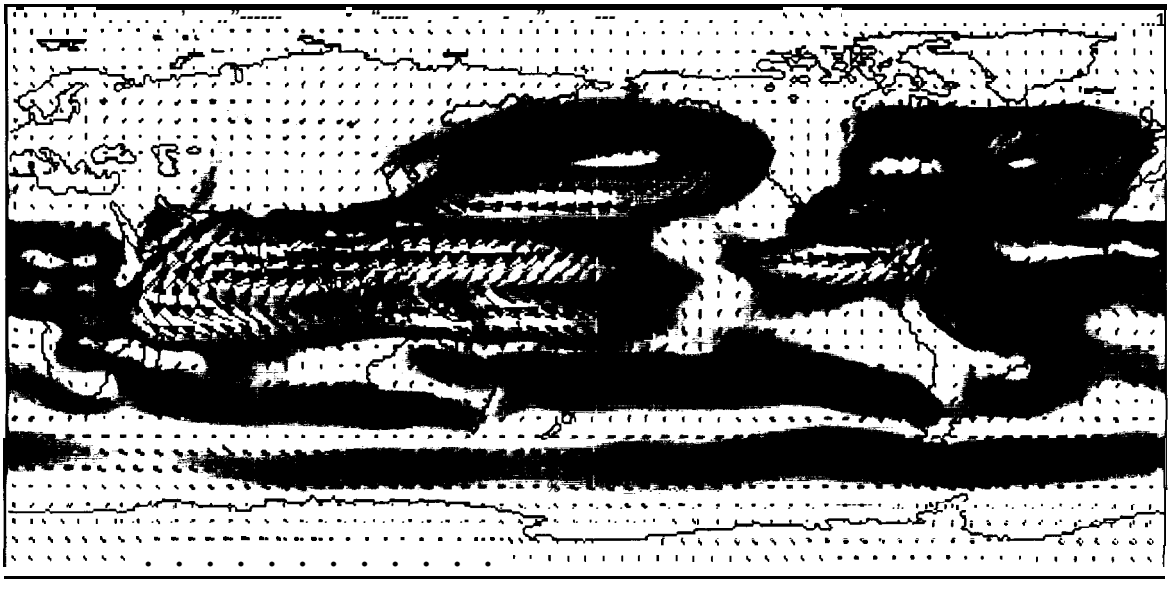

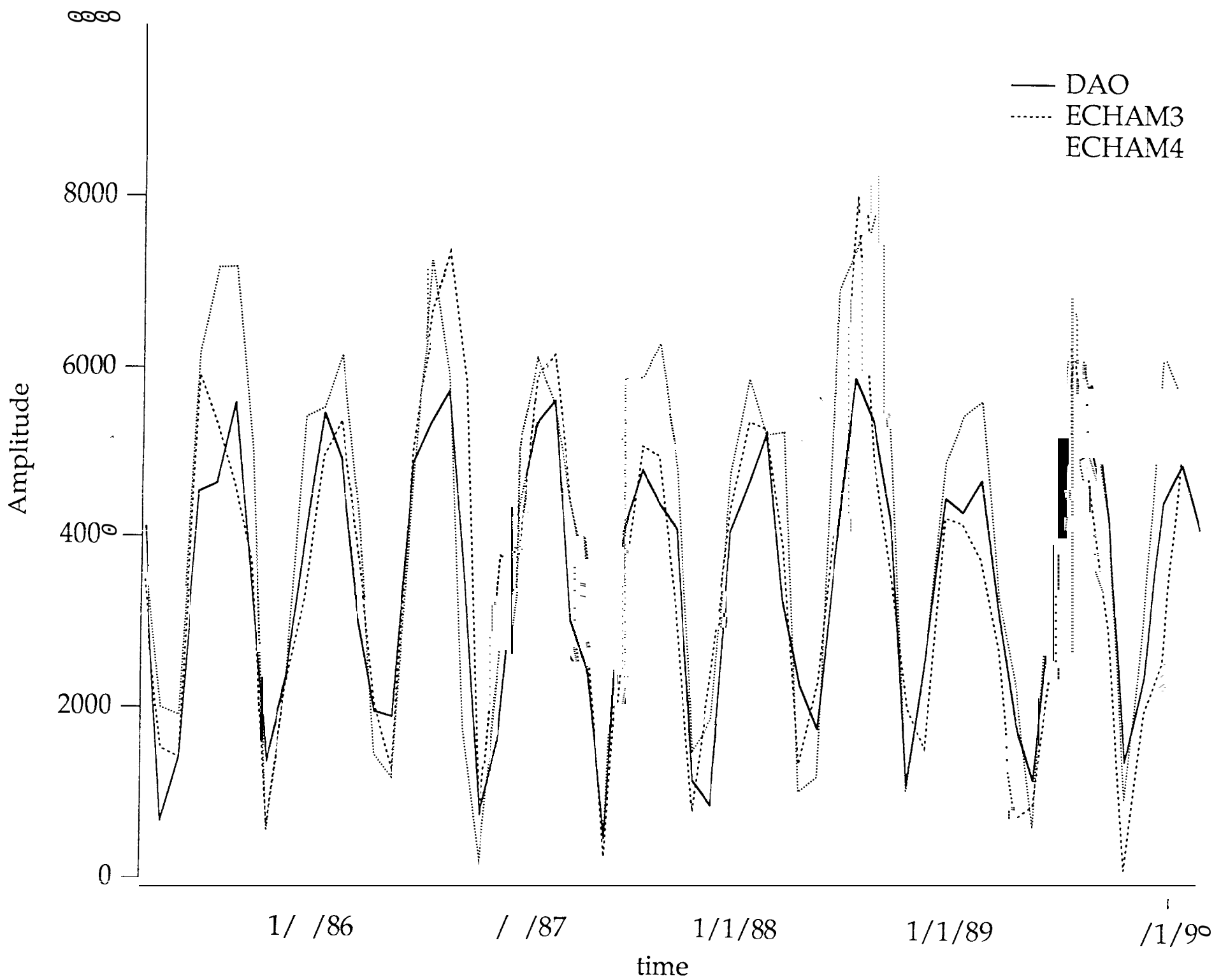
DAO
ECHAM3
ECHAM4
8000
6000
4000
2000
0
Amplitude
1/ /86
/ /87
1/1/88
1/1/89
/1/90
time

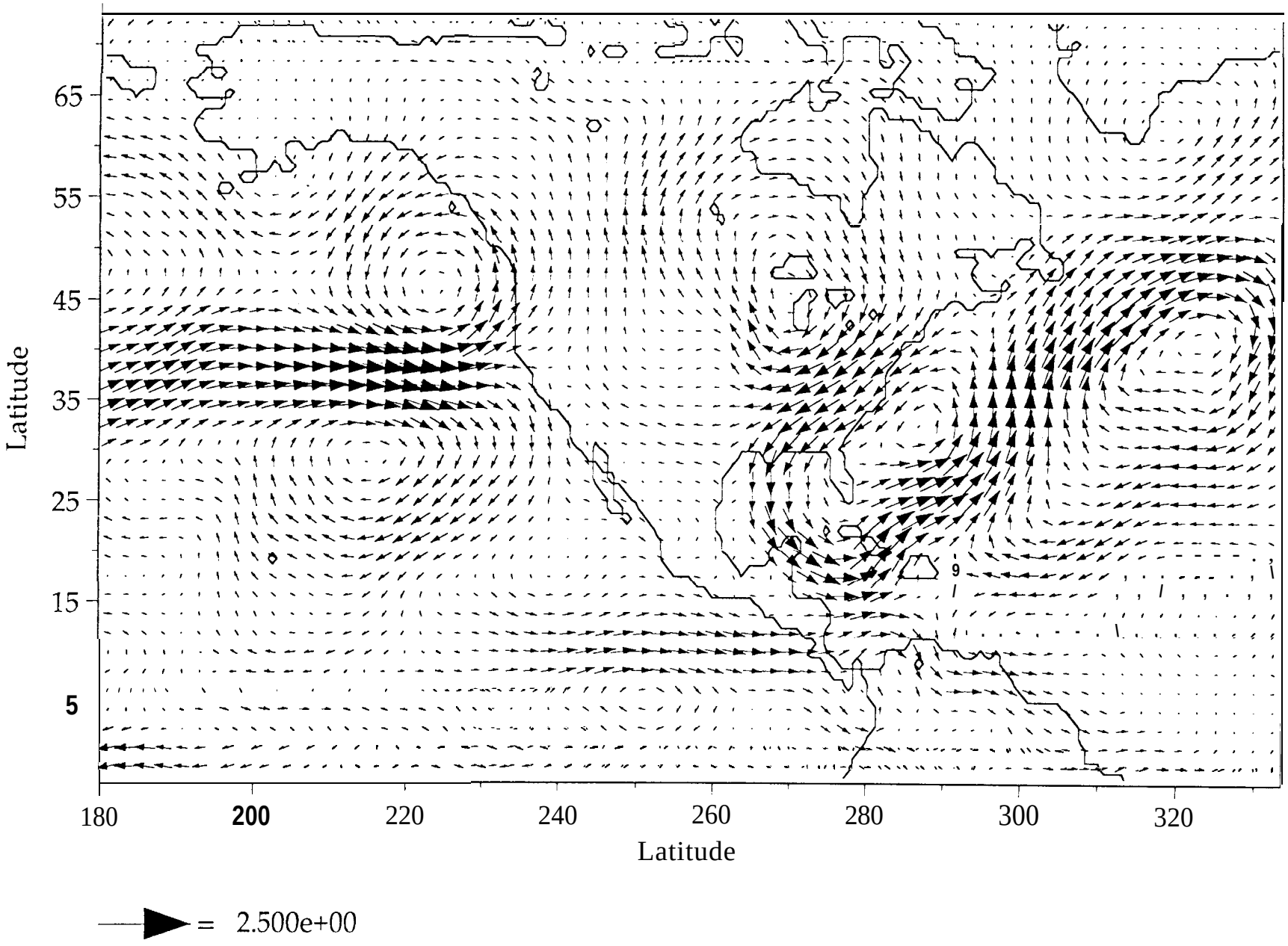
65
55
45
35
25
15
5
Latitude
180
200
220
240
260
280
300
320
Latitude
= 2.500e+00

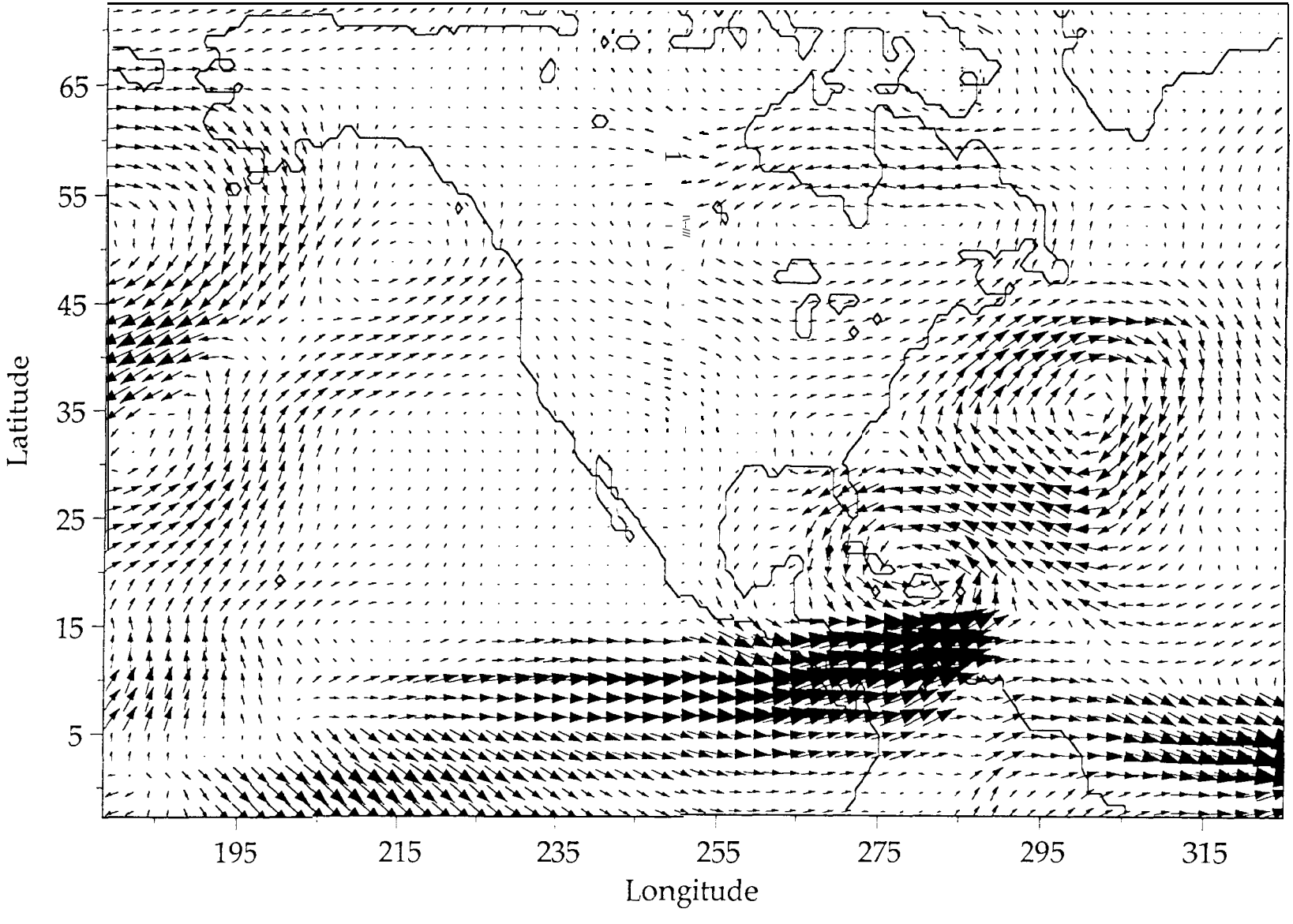
65
55
45
35
25
15
5
Latitude
195
215
235
255
275
295
315
Longitude

A = 2.500e+02

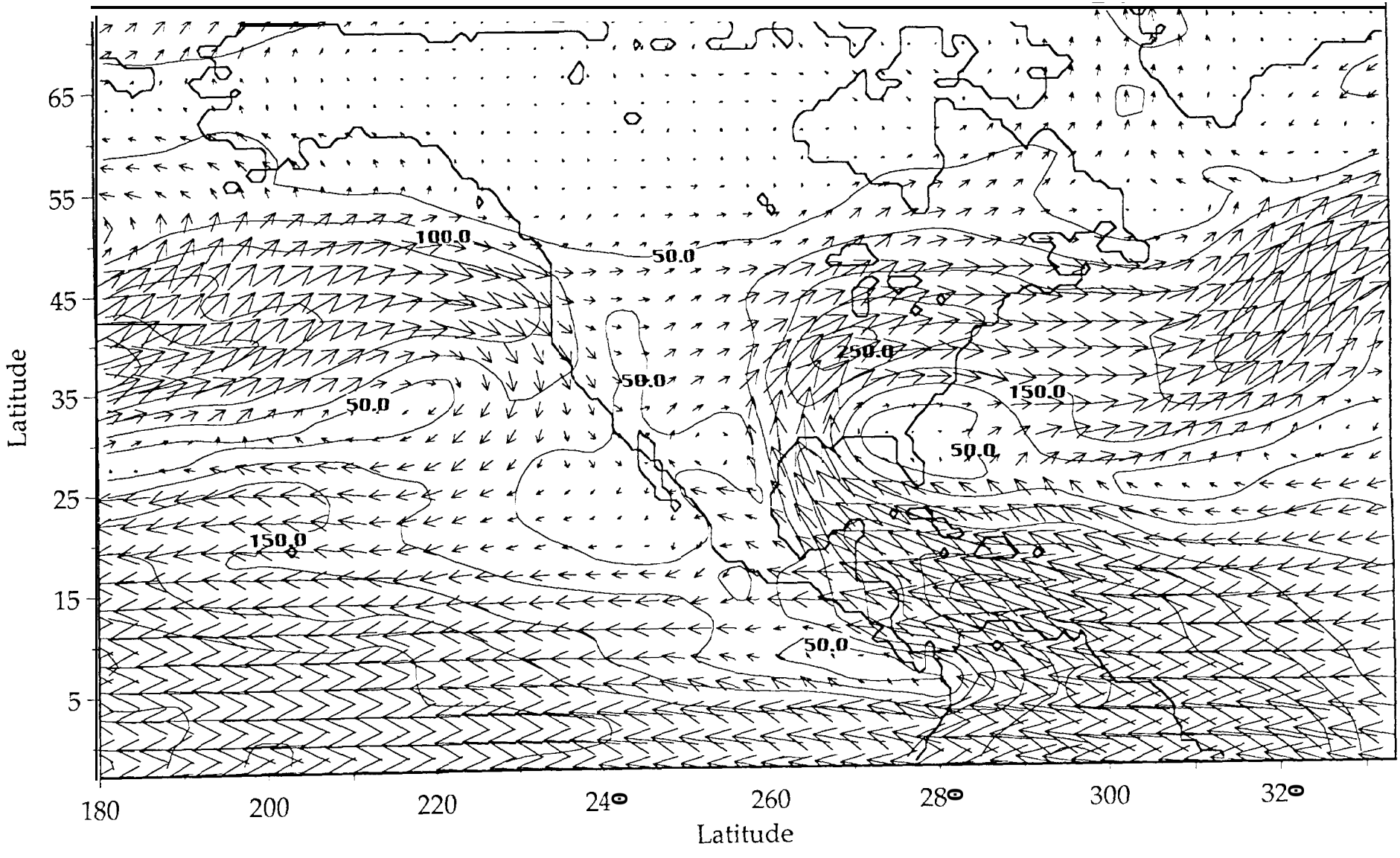
65
55
45
35
25
15
5
Latitude
100.0
50.0
50.0
250.0
150.0
50.0
50.0
150.0
50.0
180
200
220
24o
260
28o
300
32o
Latitude

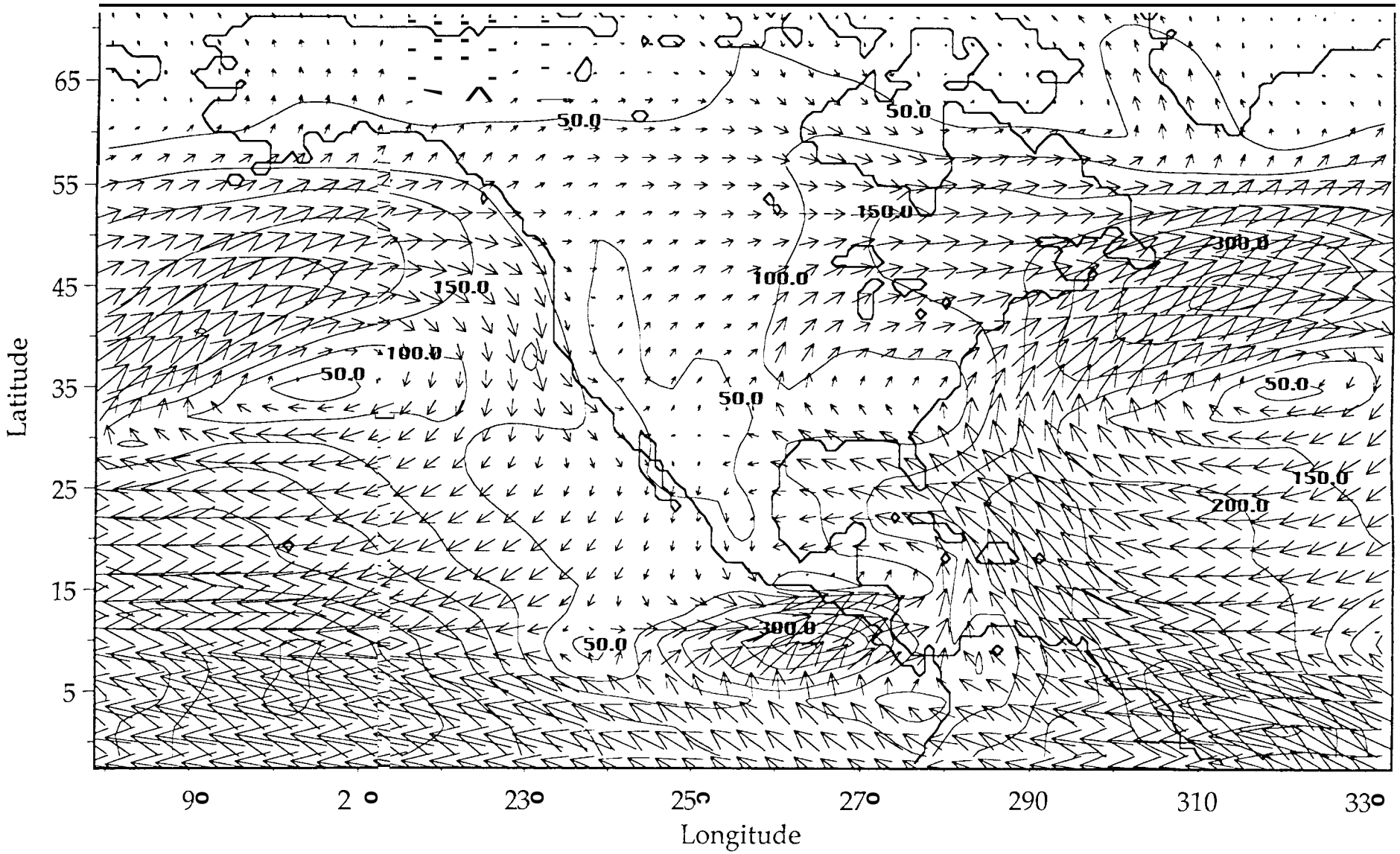
65
55
45
35
25
15
5
Latitude
90
2 0
23o
25o
27o
290
310
33o
Longitude
50.0
50.0
150.0
300.0
100.0
150.0
100.0
50.0
50.0
50.0
150.0
200.0
300.0
50.0

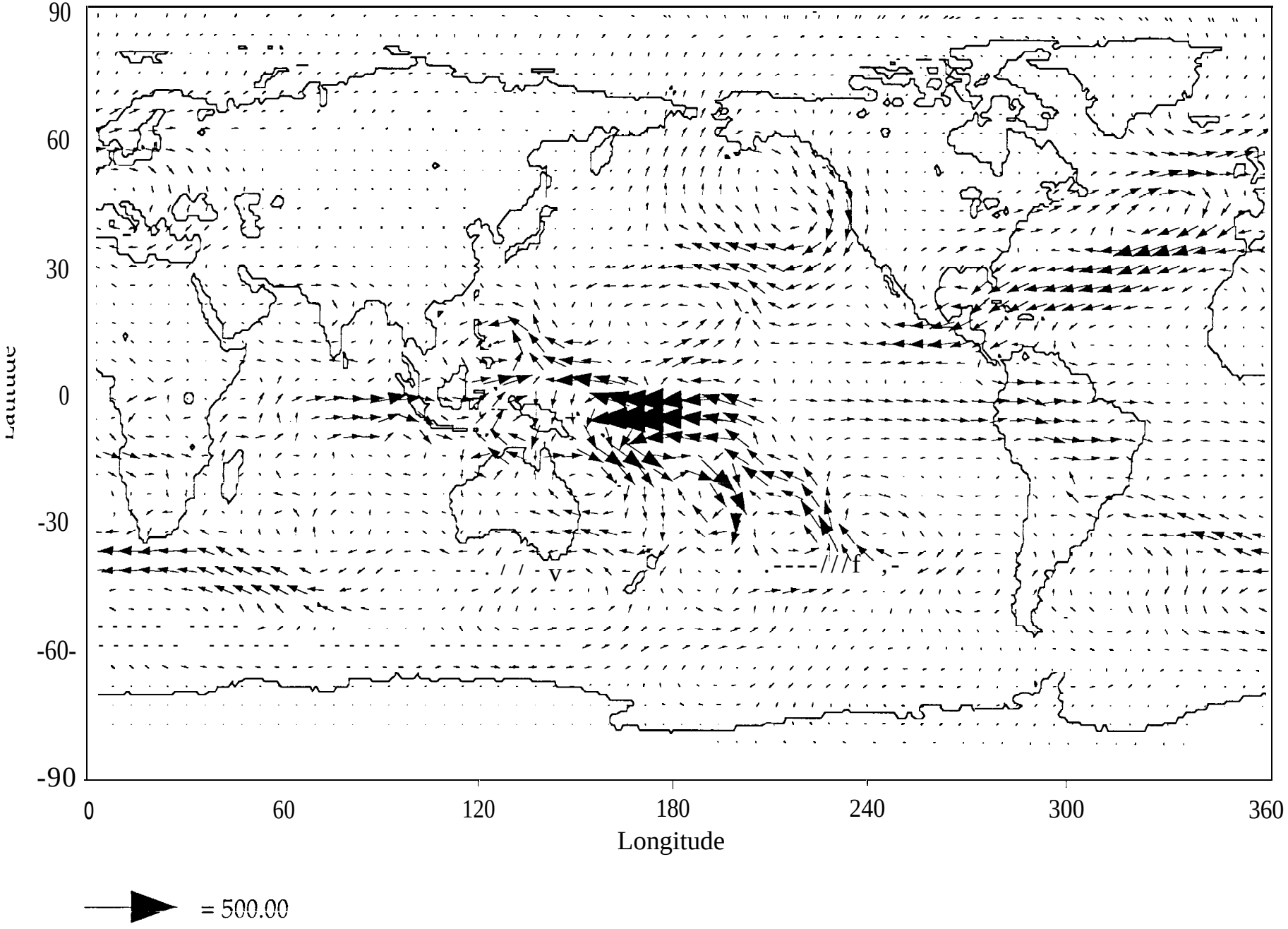
90
60
30
0
-30
-60-
-90
0
60
120
180
240
300
360
Longitude
= 500.00

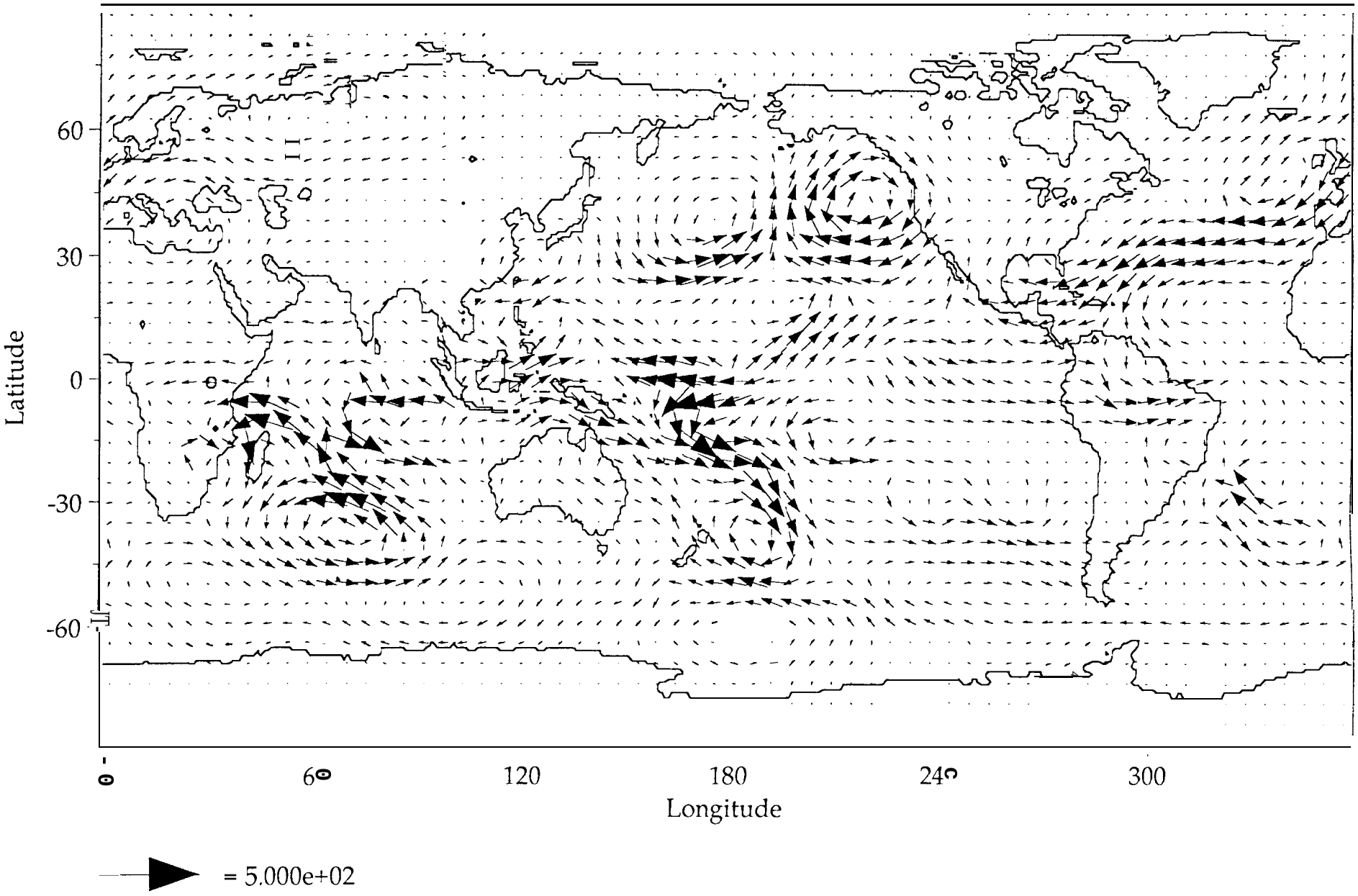
60
30
0
-30
-60
Latitude
0
60
120
180
240
300
Longitude
= 5.000e+02

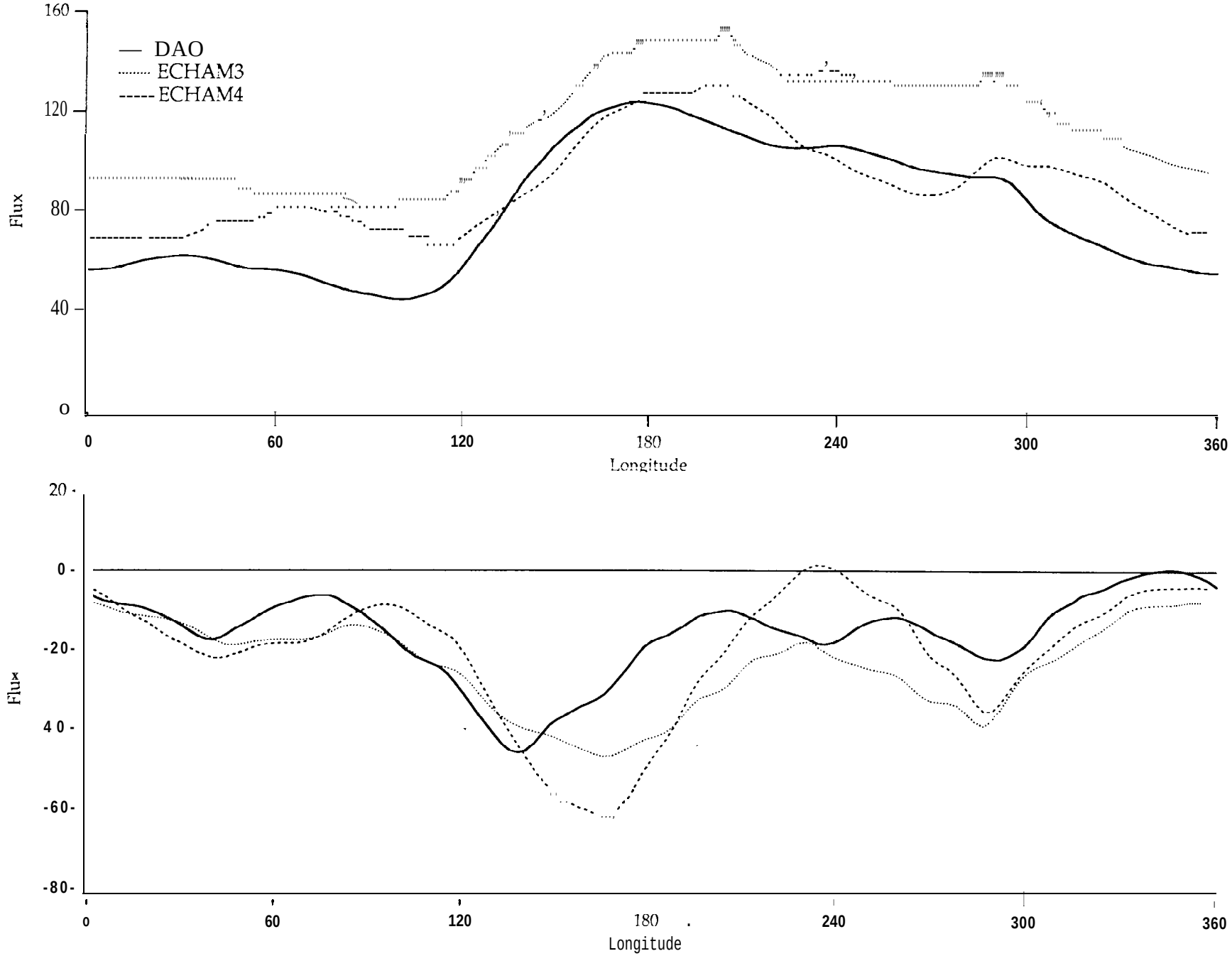
DAO
ECHAM3
ECHAM4
Flux
160
120
80
40
0
0
60
120
180
240
300
360
Longitude
20
0
-20
-40
-60
-80
Flux
0
60
120
180
240
300
360
Longitude

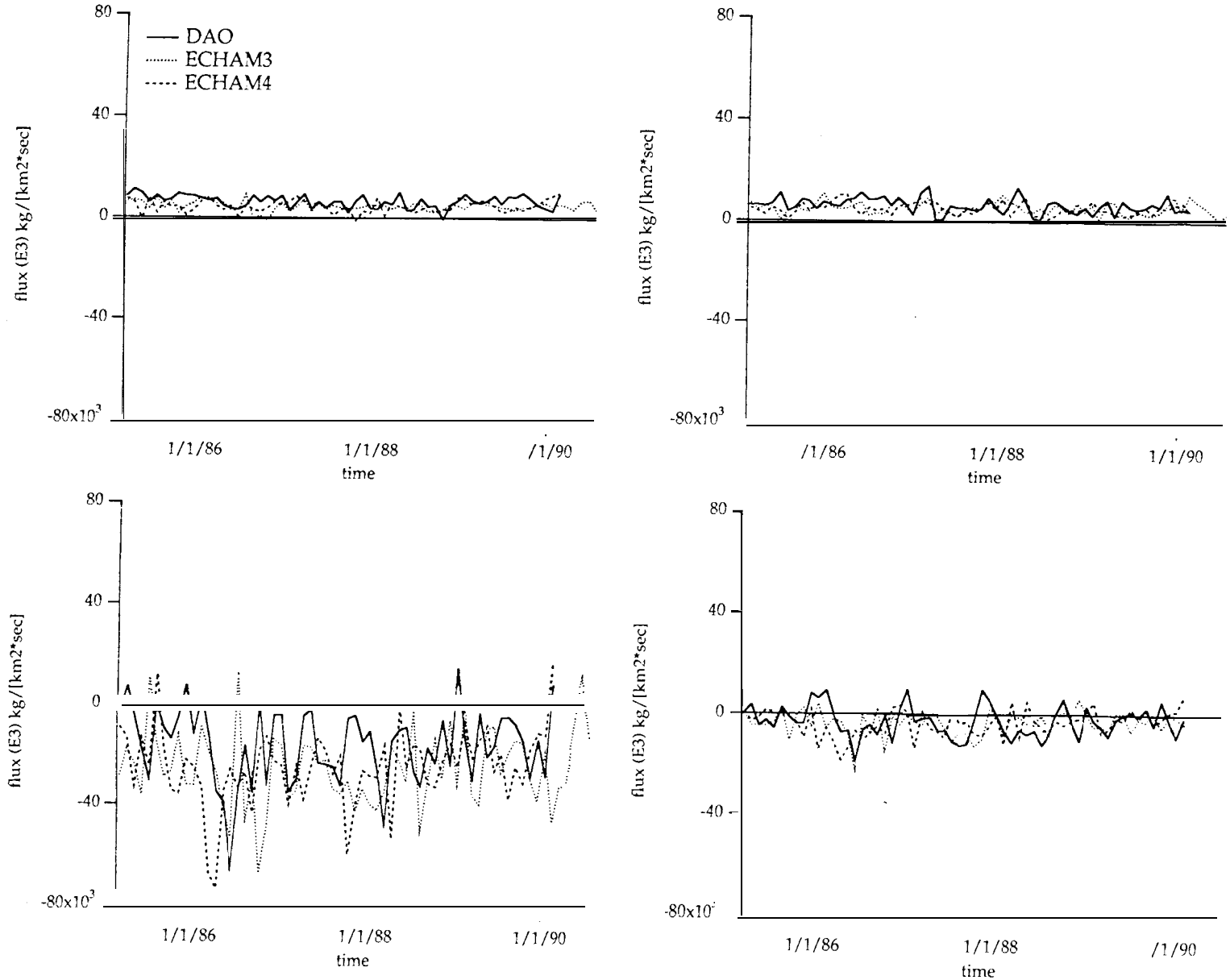
DAO
ECHAM3
ECHAM4
80
40
0
-40
-80x10^3
flux (E3) kg/[km2*sec]
1/1/86
1/1/88
/1/90
time